SANDIA REPORT

SAND2016-11572
Unlimited Release
Printed November 2016

Experiments and Computational Theory for Electrical Breakdown in Critical Components: THz Imaging of Electronic Plasmas (LDRD 173097)

Fred J Zutavern, Harold P. Hjalmarson, Verle H. Bigman, Richard J. Gallegos

Prepared by
Sandia National Laboratories
Albuquerque, New Mexico 87185 and Livermore, California 94550

Sandia National Laboratories is a multi-mission laboratory managed and operated by Sandia Corporation, a wholly owned subsidiary of Lockheed Martin Corporation, for the U.S. Department of Energy's National Nuclear Security Administration under contract DE-AC04-94AL85000.

Issued by Sandia National Laboratories, operated for the United States Department of Energy by Sandia Corporation.

Available to DOE and DOE contractors from
U.S. Department of Energy
Office of Scientific and Technical Information
P.O. Box 62
Oak Ridge, TN 37831

Telephone: (865) 576-8401
Facsimile: (865) 576-5728
E-Mail: reports@osti.gov
Online ordering: http://www.osti.gov/scitech

Available to the public from
U.S. Department of Commerce
National Technical Information Service
5301 Shawnee Rd
Alexandria, VA 22312

Telephone: (800) 553-6847
Facsimile: (703) 605-6900
E-Mail: orders@ntis.gov
Online order: http://www.ntis.gov/search

SAND2016-11572
Unlimited Release
Printed November 2016

Experiments and Computational Theory for Electrical Breakdown in Critical Components: THz Imaging of Electronic Plasmas (LDRD 173097)

Fred J Zutavern, Harold P. Hjalmarson, Verle H. Bigman, Richard J. Gallegos
5444: Laser Applications
Sandia National Laboratories
P.O. Box 5800
Albuquerque, New Mexico 87185-1153

Abstract

This report describes the development of ultra-short pulse laser (USPL) induced terahertz (THz) radiation to image electronic plasmas during electrical breakdown. The technique uses three pulses from two USPLs to (1) trigger the breakdown, (2) create a 2 picosecond (ps, 10^{-12} s), THz pulse to illuminate the breakdown, and (3) record the THz image of the breakdown. During this three year internal research program, sub-picosecond jitter timing for the lasers, THz generation, high bandwidth (BW) diagnostics, and THz image acquisition was demonstrated. High intensity THz radiation was optically-induced in a pulse-charged gallium arsenide photoconductive switch. The radiation was collected, transported, concentrated, and co-propagated through an electro-optic crystal with an 800 nm USPL pulse whose polarization was rotated due to the spatially varying electric field of the THz image. The polarization modulated USPL pulse was then passed through a polarizer and the resulting spatially varying intensity was detected in a high resolution digital camera. Single shot images had a signal to noise of ~3:1. Signal to noise was improved to ~30:1 with several experimental techniques and by averaging the THz images from ~4000 laser pulses internally and externally with the camera and the acquisition system (40 pulses per readout). THz shadows of metallic films and objects were also recorded with this system to demonstrate free-carrier absorption of the THz radiation and improve image contrast and resolution. These 2 ps THz pulses were created and resolved with 100 femtosecond (fs, 10^{-15} s) long USPL pulses. Thus this technology has the capability to time-resolve extremely fast repetitive or single shot phenomena, such as those that occur during the initiation of electrical breakdown.

The goal of imaging electrical breakdown was not reached during this three year project. However, plans to achieve this goal as part of a follow-on project are described in this document. Further modifications to improve the THz image contrast and resolution are proposed, and after they are made, images of photo-induced carriers in gallium arsenide and silicon will be acquired to evaluate image sensitivity versus carrier density. Finally electrical breakdown will be induced with the first USPL pulse, illuminated with THz radiation produced with the second USPL pulse and recorded with the third USPL pulse.

ACKNOWLEDGMENTS

The authors acknowledge the advice, suggestions, and support of Larry Schneider, David Gardner, Steve Glover, Aaron VanTassle, Tony Marrujo, James Greutzner, Ryan Law, Ray Collins, Kenn Grieves, Mark Kimmel, and many of our other colleagues at SNL, along with questions and suggestions from Daniel Mauch, a summer intern and graduate student at Texas Technical University, Lubock, TX.

CONTENTS

FIGURES

TABLES

NOMENCLATURE

BW	bandwidth
CCD	charge coupled device
CMOS	complementary metal oxide semiconductor
CPA	chirped pulse amplifier
DOE	Department of Energy
EMI	electro-magnetic interference
EO	electro-optic
EOI	electro-optic imaging
EOS	electro-optic sampling
fs	femtosecond (10^{-15} s)
GaAs	gallium arsenide
HERMES	High-Energy Radiation Megavolt Electron Source
IR	infra-red
LAC	lightning arrestor connector
LDRD	laboratory directed research and development
OAP	off-axis parabolic mirror
PCSS	photoconductive semiconductor switch
ps	picosecond (10^{-12} s)
RF	radio frequency
rms	root-mean-square
SATURN	an x-ray simulation source at SNL, MA
Si	silicon
SNL	Sandia National Laboratories
THz	terahertz
USPL	ultra-short pulse laser
WSEAT	weapons science, engineering, and technology
Z	SNL's Z-pinch machine, for high energy density experiments, MV & MA

1. INTRODUCTION

The phenomenon of electrical breakdown is important for many electrical systems and components. In general, electrical breakdown either needs to be avoided or controlled, if the system or component is going to use it. For example, lightning arresters are designed to protect electrical systems by breaking down and shorting the system when excessive voltages are encountered. Alternatively, insulators in high energy density storage, switching, and transmission systems are designed to avoid breakdown up to a pre-determined threshold.

Predictive modeling of electrical breakdown is important for evaluating the threat of lightning strikes on systems and components, and characterizing electrical breakdown in the components of all types of high voltage systems. Predicting the probability of electrical breakdown is particularly critical at SNL for high voltage systems such as firesets, lasers, high energy density science experimental facilities (Z, HERMES, and SATURN), high power RF and microwave generation, and optically induced plasma radiation (RF-THz regime). However, electrical breakdown modeling is not very accurate, particularly as the complexity of the system increases. Science-based modeling of electrical breakdown has had limited success in predicting many of the observed characteristics, including probability of breakdown as a function of electric field, the location and size of primary current channels, damage on solid surfaces and in bulk insulating and multi-phase materials, the generation and relative roles of ion and electron distributions in initiating and growing an electrical discharge, and the interaction with solid interfaces near breakdown events without the help of well diagnosed and discovery experiments[1,2].

Part of the basic problem for modeling electrical breakdown is its stochastic nature (an extremely large number of particles are involved) and the number of paths or mechanisms through which these particles can participate in the initiation of electrical breakdown. Evaluating the probabilities of a multiple path problem requires critical information about all of the possible paths. The goal of this project was to develop a new experimental technology to provide critical missing information about the initiation of electrical breakdown and thereby improve the predictive capability of electrical breakdown models.

The specific plan for this research was to develop a new plasma diagnostic that will provide information about the spatial distribution of electronic plasma (electrons with or without ions) during the initiation of electrical breakdown. Visible photographs of electrical breakdown (Figure 1) show the distributions of electrons and ions as they recombine and emit visible radiation. However, in situations where electrons and ions are separated, recombination is not possible and these photographs provide no information about the charge distributions. Visible light does not interact strongly with electronic densities that are prevalent during the initiation of electrical breakdown which are typically in the range of 10^{10}-10^{20} cm^{-3}. However, longer wavelength radiation (30 to 300 μm or 10 to 1 THz) excites plasma oscillations in the middle of this electron density range[3]. The idea behind this new plasma diagnostic is to use radiation in the 1-10 THz regime like a photographer's flood lamp to illuminate and to create images of the electronic plasma during the initiation of electrical breakdown. Then by comparing the THz images with visible (recombination) images, the distribution of isolated electronic plasma may be evaluated.

What happens first, as the channels form along the dielectric in Figure 1 [4,13]? Does ionization occur near the bright tip of the upper discharge and grow into fine filaments, or are electrons emitted that scatter off the high dielectric surface creating more electrons which eventually gain enough energy from the electric field to ionize the gas near the surface? Perhaps a simpler experiment could answer this question, if an image of the electronic plasma could be recorded as a function of time. Fast frame visible images may be able to show the time evolution of electron-ion recombination, but they won't show the initial distributions of electrons which are much more mobile than the ions.

Figure 1. This photograph is an open shutter picture of surface flashover near the high dielectric material used in lightning arrestor connectors (LAC). The event was triggered with a fine wire near the top of the dielectric stack. This picture was taken by Zachariah Wallace for Jane Lehr [4,13].

2. TERAHERTZ RADIATION AND ELECTRONIC PLASMAS

The problem with recording images of the electron distributions during the initiation of electrical breakdown is that visible or near-visible light does not interact strongly with these carrier densities of elections. Light is strongly absorbed and reflected from metals, because their carrier densities are much higher, e.g. copper has a nearly-free electron density of 10^{23} cm^{-3}. The plasmons that form in copper absorb in the blue producing the red-orange color that is observed when copper reflects white light.

2.1. Plasma Frequencies and Carrier Densities

A uniform density of free electrons will oscillate at a plasma frequency given by:

$$\omega_{pe} = \sqrt{\frac{n_e e^2}{m^* \varepsilon_0}}, [rad/s] \quad \text{(SI units)} \qquad (1)$$

$$f_{pe} \approx 8980\sqrt{n_e} \quad \text{(Hz, cm}^{-3}\text{)} \qquad (2)$$

where f_{pe} is the plasma frequency, ω_{pe} is the angular plasma frequency of electronic carrier density, n_e, with charge, e, effective mass, m^*, and dielectric constant of free space, ε_0 [3].

2.2. Optimum Radiation for Imaging is USPL-induced THz radiation

Table I shows the plasma frequencies from equations (1) and (2) corresponding to electronic plasma densities which are characteristic of electrical breakdown. The electromagnetic radiation corresponding to these frequencies ranges from 10 GHz to 10 THz is far below visible, in the terahertz regime and lower. In fact, the sudden creation these carrier densities with an USPL will produce plasma radiation in this regime. Similar to black body radiation, good absorbers will be good emitters and vice versa. Thus THz radiation is the ideal radiation for imaging the electronic plasmas during the initiation of electrical breakdown and USPL-induced THz is produced in short pulses (~ 1 ps) which are ideal for imaging high speed phenomena.

Table 1. Electronic Plasma Frequency

Frequency (GHz)	Free electron density (cm^{-3})
10,000	1.240×10^{18}
1,000	1.240×10^{16}
100	1.240×10^{14}
10	1.240×10^{12}

The plasmas created during electrical breakdown are not uniform density as shown in Figure 1. Their emitted radiation and interaction with incident electromagnetic radiation will be much richer in bandwidth than monochromatic plasma frequency radiation. It should be noted that microwaves have been used to characterize low density plasmas. The advantages of using broadband radiation (10 GHz - 10 THz or 3 cm - 30 μm) are stronger interaction with higher density plasmas and shorter wavelength components that will have higher spatial resolution. This is similar to imaging objects with white light as opposed to a single color.

2.3 Characteristics of USPL-induced THz Radiation

Electro-optic sampling (EOS) measurements of the time-dependent intensity of USPL-induced THz radiation from a GaAs PCSS are shown in Figure 2. EOS measures the polarization rotation of short optical pulses that are co-propagated with the THz wave in an EO crystal [5, 10]. Thicker EO crystals provide more sensitivity and thinner crystals provide higher bandwidth due to dispersion between the optical and THz radiation. The thickness of the zinc telluride (ZnTe) crystal used in these measurements was 4 mm. Measurements with 100 µm crystals have shown USPL-induced THz radiation with bandwidths greater than 10 THz. The bandwidth-limited measurement (Figure 2) of the time between the positive and negative peaks in the bipolar pulse of THz radiation is 1 ps. This pulse was created with a 100 fs pulse from a USPL. This extremely short burst of THz radiation allows time resolution of ultra-short phenomena, but also requires extremely precise timing from the supporting sub-systems for electro-optic imaging (EOI). Timing techniques will be described briefly in the next sections.

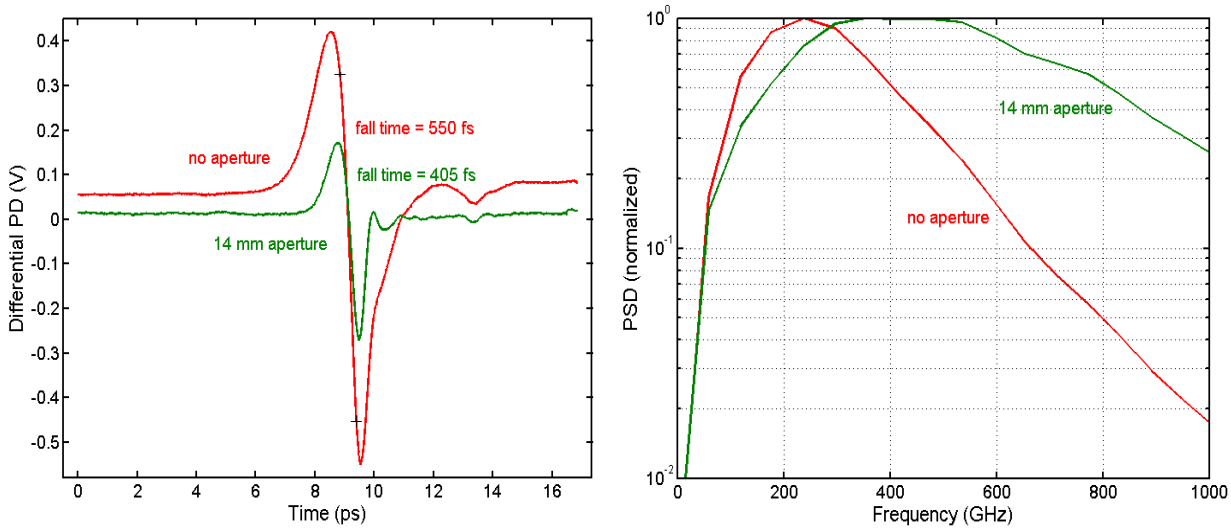

Figure 2. A comparison of time domain signals measured with EOS (left) and frequency domain Fourier transform power spectral densities (right) is shown for 100 fs USPL-induced THz in a GaAs PCSS. Bandwidth of the EOS diagnostic was improved by inserting a 14 mm aperture between the 50 mm diameter parabolic THz mirrors used to collect and focus the THz beam into a ZnTe EO crystal. Fall times decreased (left) and the 3 dB point increased from 400 to 800 GHz (right). EOS is a pump-probe technique that measures the amplitude of the THz pulse versus time by varying the optical path length of the probe pulse relative to the THz.

A picture of the EOS optics is shown in Figure 3. This technique is similar to EOI in many ways, but the biggest difference is that EOS uses a matched pair of differential photo-diodes to record extremely low-noise changes in the polarization of the optical probe pulse from the total burst of THz radiation co-propagating through the EO crystal at a specific point in time. EOI, on the other hand, resolves the THz intensity variation in space by imaging the optical probe pulse through a crossed polarizer onto a high resolution camera with the equivalent of millions of photo-diodes. The biggest issue with EOI is the ratio of signal to noise. The large number of pixels and the weak signal from the EO polarization rotation make this diagnostic very challenging. The USPL operating characteristics and diagnostics used to measure them are listed in Table 2.

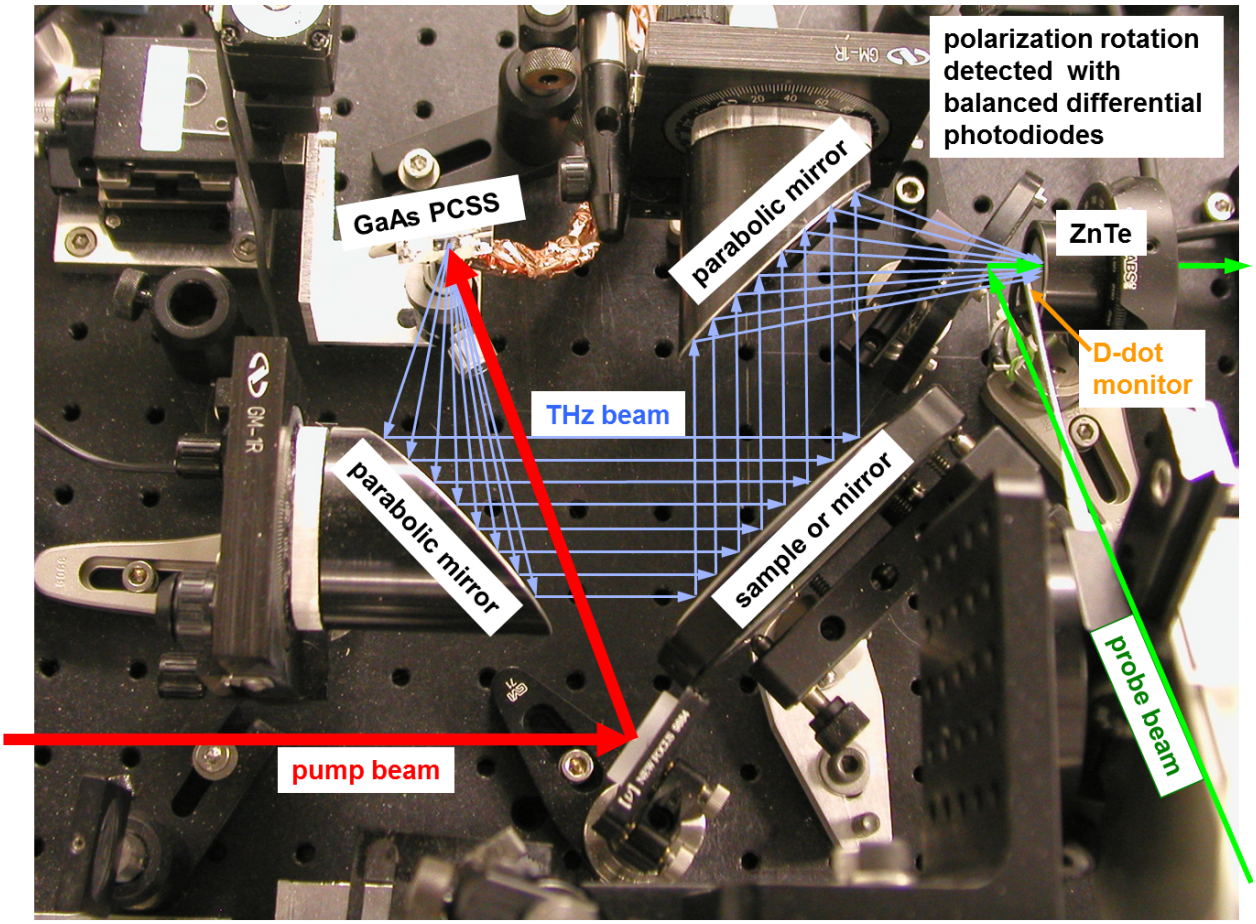

Figure 3. This photograph of EOS shows the optical components that collect, collimate, and concentrate THz radiation (blue) from a USPL pulse (red) onto a GaAs PCSS. The THz radiation is focused into a ZnTe EO crystal to measure the average spatial intensity with a co-propagating probe beam (green).

Table 2. USPL Diagnostics and Characteristics

Energy	Power Meter/Repetition Rate	1 mJ
Pulse Width	Single Shot Auto-correlator	65 fs
Wavelength	Spectrometer	15 nm @ 800 nm
Near Feld Image	High Resolution Camera	Gaussian Profile
Far Field Image	Far Field Optics + Hi Res Camera	Gaussian Profile
Chirp	Freq. Resolved Opt. Gate (FROG)	Low Spatial Chirp
Jitter	40 MHz Photodiode	3 ps
THz Field	D-dot & EOS	100 V/cm

3. THE THREE USPL PULSE EXPERIMENT

This experiment creates three pulses from an 800 nm ultra-short pulse laser system to: (1) trigger an electrical breakdown event, (2) initiate a 1 ps pulse of THz radiation, and (3) to convert the THz image to an 800 nm, near infra-red (IR) image. The laser system consists of an 80 MHz, 60 fs, seed laser and two 1 kHz regenerative chirped-pulse amplifiers (CPA). Two amplifiers are used so that different seed pulses may be amplified and their time separation may be large to trigger electrical breakdown well in advance of the THz source and the image conversion.

A diagram of the multiple-pulse laser configuration is shown in Figure 4. The first pulse, which comes from the bottom amplifier, can trigger electrical breakdown at two locations so images may be acquired in either transmission or reflection. The pulse from the second amplifier is split into the second and third pulses. The second pulse creates a sudden electron-hole plasma which is the source of the THz radiation. It is collected and collimated with an off-axis parabolic (OAP) mirror. This collimated THz beam is incident on the electrical breakdown event. The transmitted or reflected THz radiation is collected with another OAP after interacting with the electrical breakdown event. The second OAP focuses the THz through a transparent pellicle into an electro-optic (EO) crystal. Simultaneously, the third USPL pulse, which is linearly polarized, reflects off the pellicle and co-propagates with the THz image.

The spatially varying electric field from the THz image rotates the polarization of the co-propagating 800 nm pulse. After passing through a crossed polarizer, the 800 nm pulse contains the spatial intensity modulations that correspond to the THz image. The modulated 800 nm pulse is imaged onto a camera, and recorded as a copy of the THz image from the electrical breakdown event. This USPL pulse-probe imaging technique is commonly known as EO imaging [5-8].

A photograph of the lasers and THz source and imaging optics is shown in Figure 5

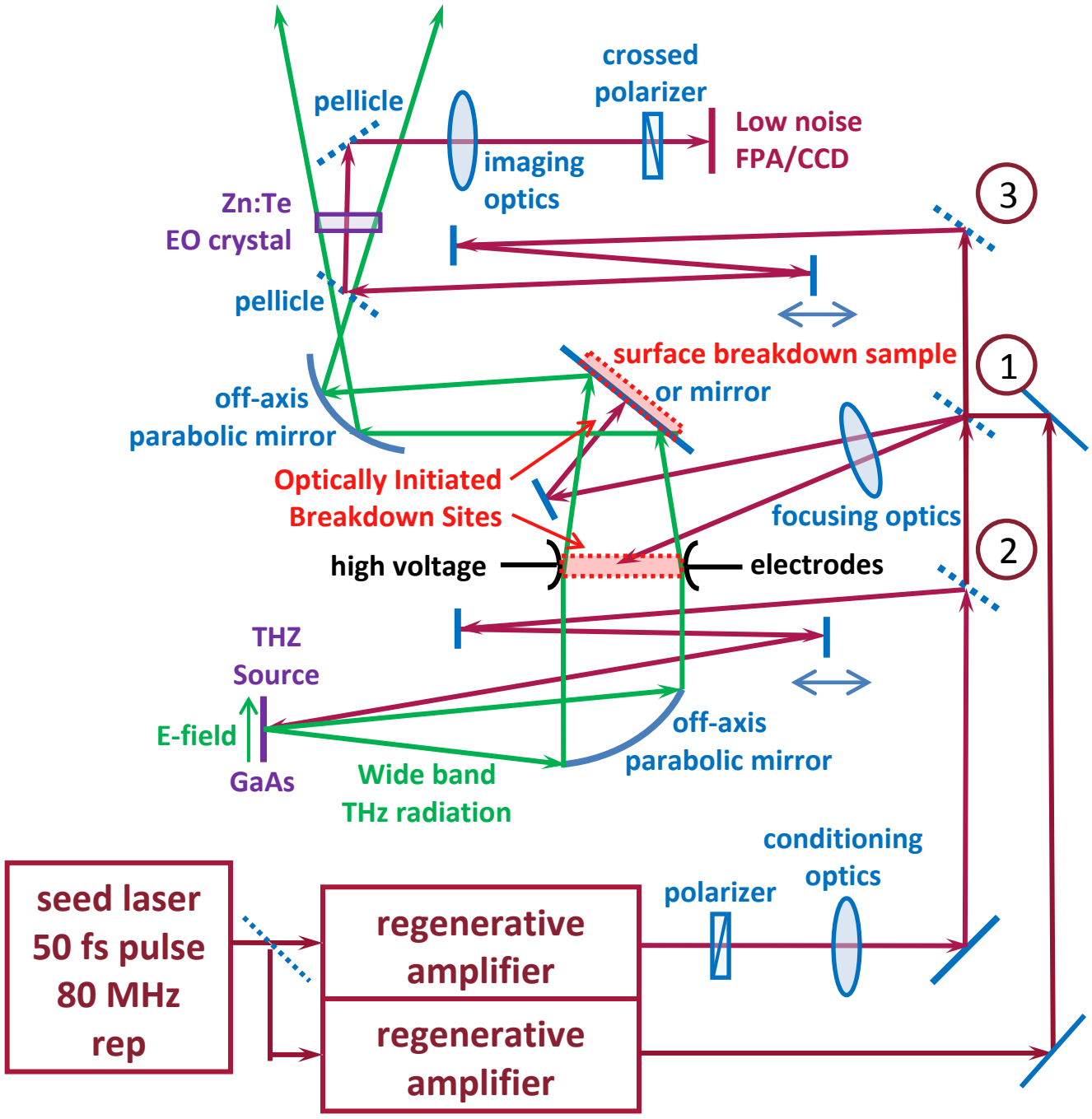

Figure 4. This diagram shows how 3 USPL pulses are used to image electrical breakdown with pulsed THz radiation. The THz radiation illuminates an electrical breakdown event. Then the radiation from the breakdown is collected and converted to an 800 nm image with an EO crystal and recorded with a high resolution silicon camera.

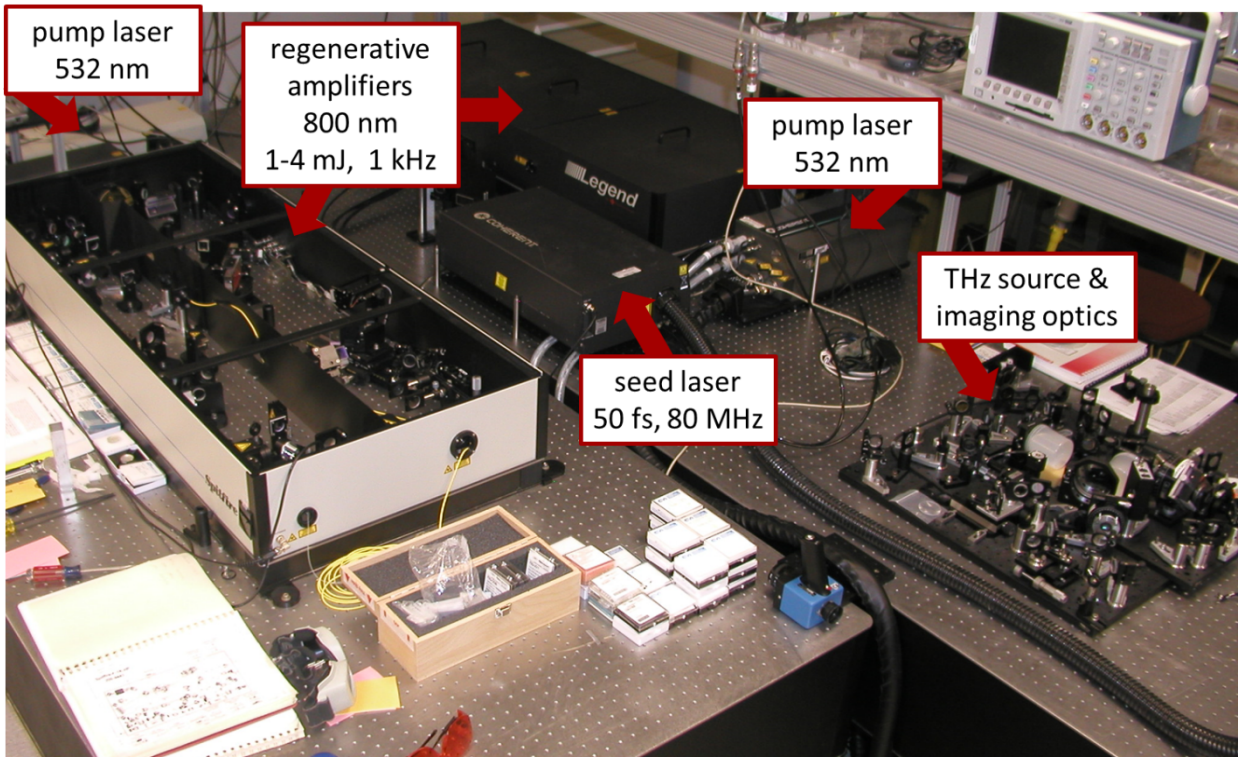

Figure 5. The seed laser, regenerative amplifiers, and the THz source and imaging optics are shown in this photograph. The system sits on adjoining 4' X 8' and 4' X 10' optical tables.

4. TIMING: LASER, PULSER, DIAGNOSTICS, & IMAGE ACQUISITION

Timing is a critical and complicated component of USPL-induced pulsed THz imaging. Due to the need for relatively long delays between triggering and imaging a breakdown event, two regenerative amplifiers are used with the ability to amplify independent pulses from the seed laser. In this way (see Figure 6), the time between the breakdown trigger pulse and the THz pump and probe pulses is adjustable to much longer time delays than are practical with path length variations (1ns/ft).

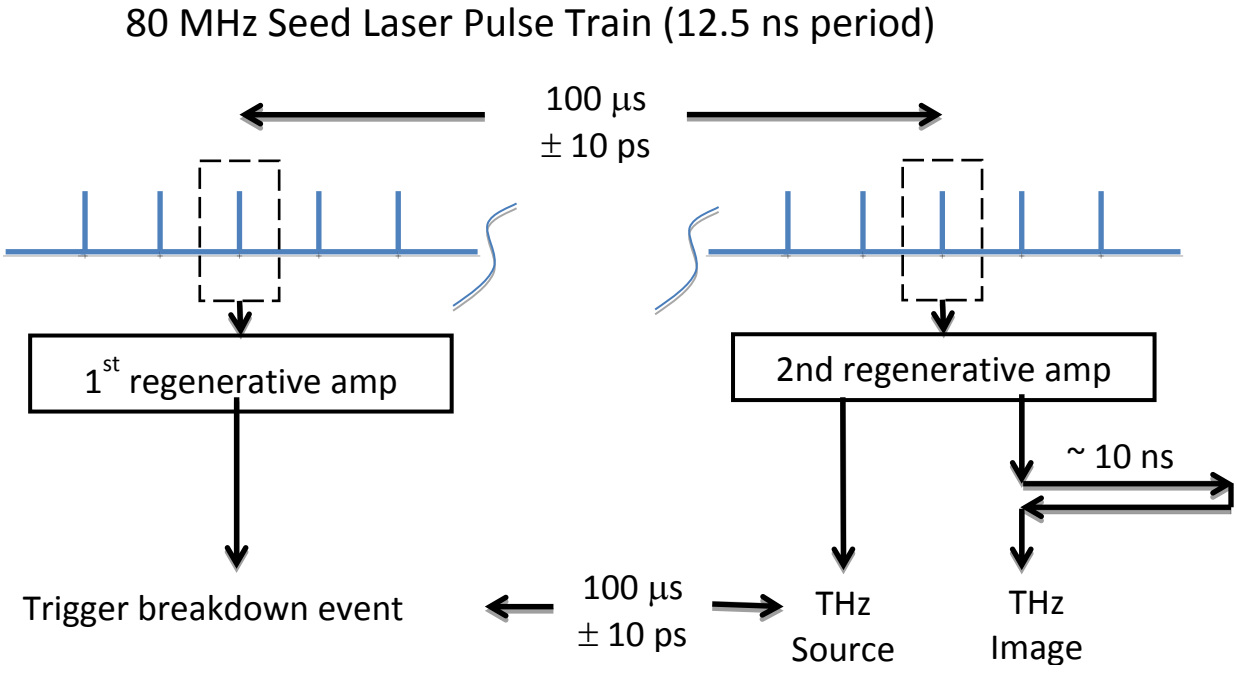

Figure 6. This timing diagram illustrates how two different pulses from the seed laser are selected for amplification by the two regenerative amplifiers to get greater time separation than is practical with path length variations (1 ns/ft). The seed laser cavity is very stable, but cavity length variations of 300 µm will produce a 2 ps time variation.

The time variation between independent pulses from the seed laser depends on the stability of the seed laser cavity. Figure 7 shows the results of a measurement between two pulses from the seed laser amplified by two separate laser amps. In this example, the rms jitter was 3.4 ps, which is certainly low enough to resolve sub-nanosecond components of electrical breakdown. However, the high bandwidth diagnostics required for monitoring laser operation and THz generation require jitter less than 5 ps. For example, a 70 GHz sampling scope requires a 30 ns pre-trigger from the 1 kHz rep-rate laser system for each sample of the measurement to build a reliable picture of the time-varying waveform. For this trigger, an RF switch is used to select a specific pulse from the seed laser to trigger the sampling scope in advance of the pulse that it is recording. This is similar to the technique used to trigger electrical breakdown in advance of the pump and probe pulses used for imaging the electrical breakdown (Figure 6).

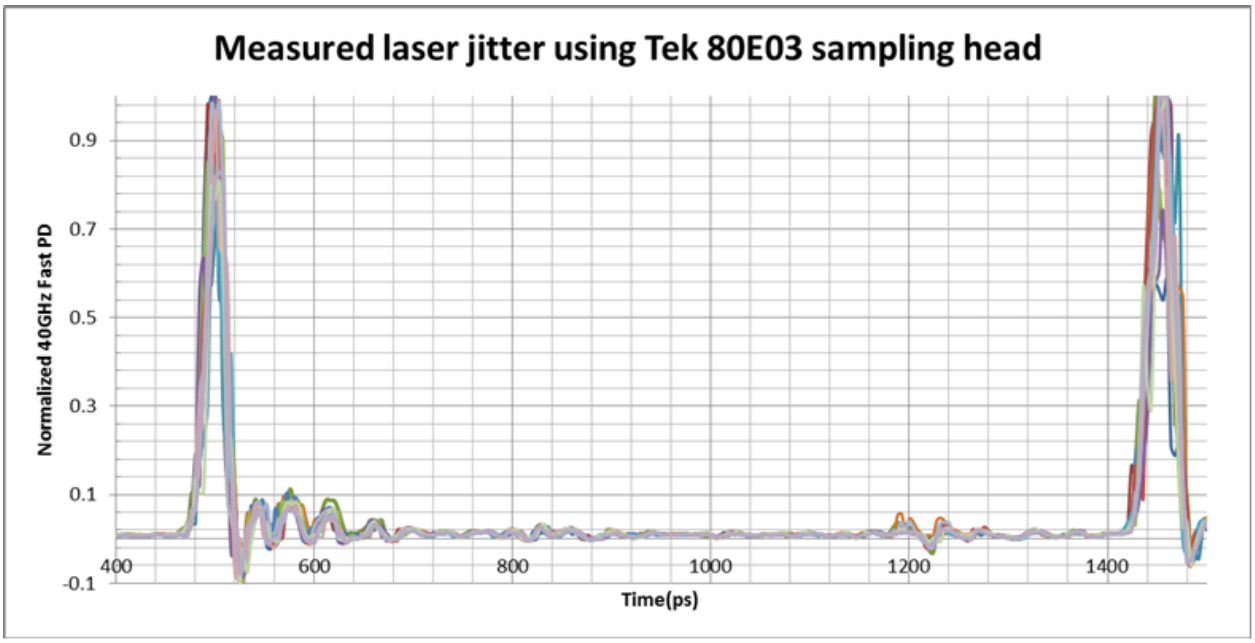

Figure 7. The time variation between two pulses from the seed laser was measured repetitively in this oscilloscope display. The root-mean-square (rms) jitter was 3.4 ps with 11 ps spread in 16 samples. Path lengths of these two pulses were adjusted to bring them closer together for this measurement.

The subsystems of this experiment also require precision timing signals which are derived from the 80 MHz seed laser. Figure 8 shows the array of timing generators used to control the lasers, the THz pulser, the diagnostics, and the image acquisition. A block diagram with the progression of the timing control from the seed laser to the major sub-system components is shown in Figure 9. The regenerative amplifiers operate at 1 kHz, so the experiment basically repeats at that rate. For improved signal-to-noise, images from the 1 kHz events are often averaged internal in the camera to reduce the effects of readout noise and random laser variation. For example the images from 40 laser pulses will be averaged in the camera in 40 ms. Then the readout to the computer buffer can take up to 30 ms. An efficient THz source requires a high electric field across the PCSS. This field is delivered to the PCSS through a high voltage, high bandwidth cable in 100 ns pulses from a 1 kHz repetition rate, 10 kV, 50 ns rise-time pulser.

Images are always recorded with THz "on" (signal) and THz "off" (background) by gating the pulser trigger and the laser amplifiers to create a burst of pulses to integrate the signal in the camera, wait for the readout into a signal buffer, then a burst of pulses to integrate the background in the camera, and then wait for the read-out into a background buffer. Background and signal images are automatically acquired to remove the systematic errors caused by non-zero crossed polarizer extinction, crystal defects, and camera dark current. Laser pulses are supplied during the integration times of both signal and background, but not during the readouts. The real-time result of signal minus background image buffers is displayed at a monitor so the operator can adjust the lasers and optics to optimize the signal. Presently, with 14 bit digitization in the camera, the near saturation signal and background images are ~14,000 counts their difference is only a few 100 counts, or a few percent of the original images. Once the system is optimized to acquire images, they are saved to disk as raw signal and background images. To

allow for the time delay caused by writing the images to disk, the signal and background images are presently being saved at 5-10 Hz. Sets of 100 or more signal and background pairs are saved in a few seconds. Then they are subtracted and averaged off-line to obtain a further increase in sign-to-noise and measure the image statistics. The background in the resulting average of a set of 100 pairs is typically 10-15 counts and the peak signal is 300-500 counts, so the final signal-to-noise is typically 30. When the first discernable THz images were recorded, signal-to-noise was about 2:1. The techniques to achieve this improvement will be described in section "7. Imaging Improvements."

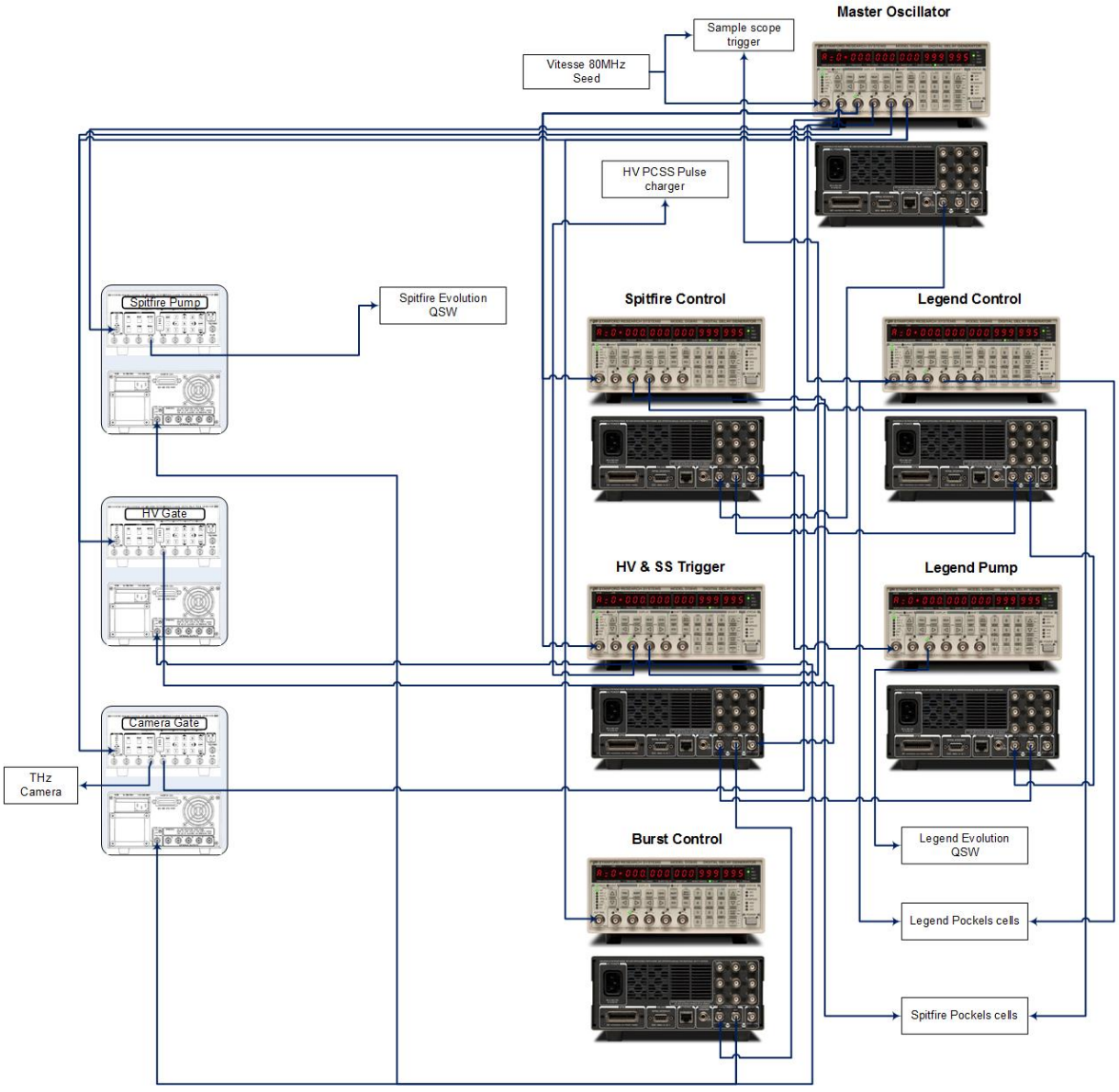

Figure 8. This diagram shows the nine digital delay generators that are used to control the lasers, diagnostics, THz pulser, and image acquisition.

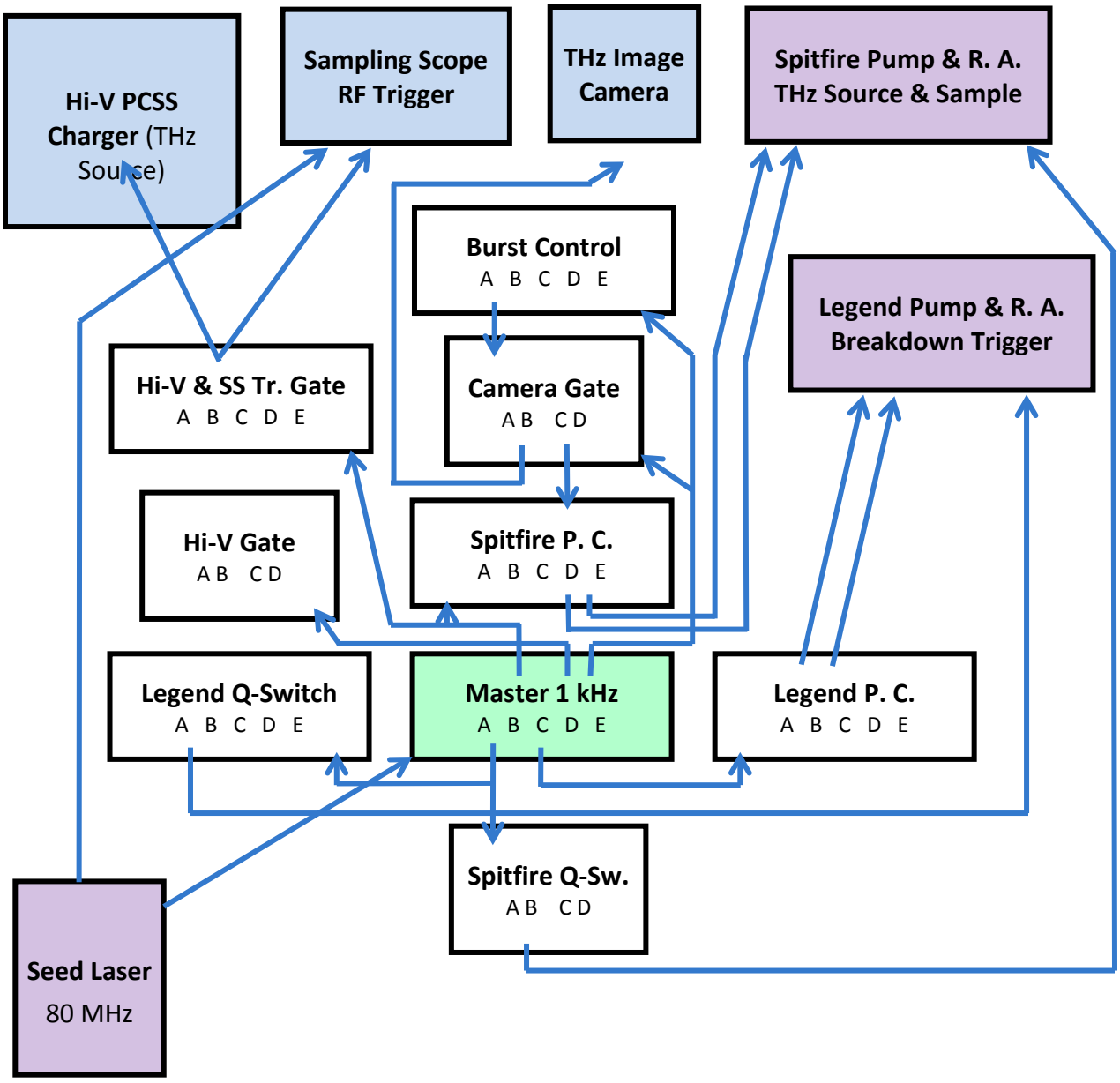

Figure 9. This block diagram shows the timing control progression from the 80MHz seed laser to the other components. All systems are synchronized to the 80 MHz seed laser with a phase locked loop on the rubidium clock in the master delay generator.

5. THZ GENERATION AND DETECTION

Plasma radiation is generated whenever an intense USPL is focused into any material, including air [10-12]. The high electric field of the laser pulse ionizes and ablates materials so rapidly that the accelerated charged particles radiate an extremely short pulse with very wide bandwidth (Figure 2). A photograph of some of the observable phenomena associated with the sudden creation of plasma is shown in Figure 10. Plasma radiation is also produced when an electron-hole plasma is generated suddenly in a semiconductor. An applied electric field increases the charge acceleration and hence intensity of the radiation as shown in Figure 11 and Figure 12. From Figure 11, RF-THz production takes nearly 6 orders of magnitude less laser intensity in a semiconductor with an applied field than in other zero field materials. For this reason, a GaAs PCSS with an applied field is used to generate the pulsed THz for this THz imaging project.

THz radiation can be detected with EOS as described in section

2.3 Characteristics of USPL-induced THz Radiation." It can also be detected with RF monitors such as RF horns and D-dots, which measure the derivative of the incident electric field. The limitation of RF monitors, when compared with EOS is their bandwidth, which is normally only a few GHz to 10s of GHz. However, the extremely wide band spectrum of USPL-induced THz, provides a significant signal in these lower spectral regimes. Often considered noise, the low frequency part of the spectrum is sufficient to characterize the amplitude of the emission as shown in Figure 11, where measurements from a 65 GHz BW D-dot are compared to the 500 GHz BW EOS.

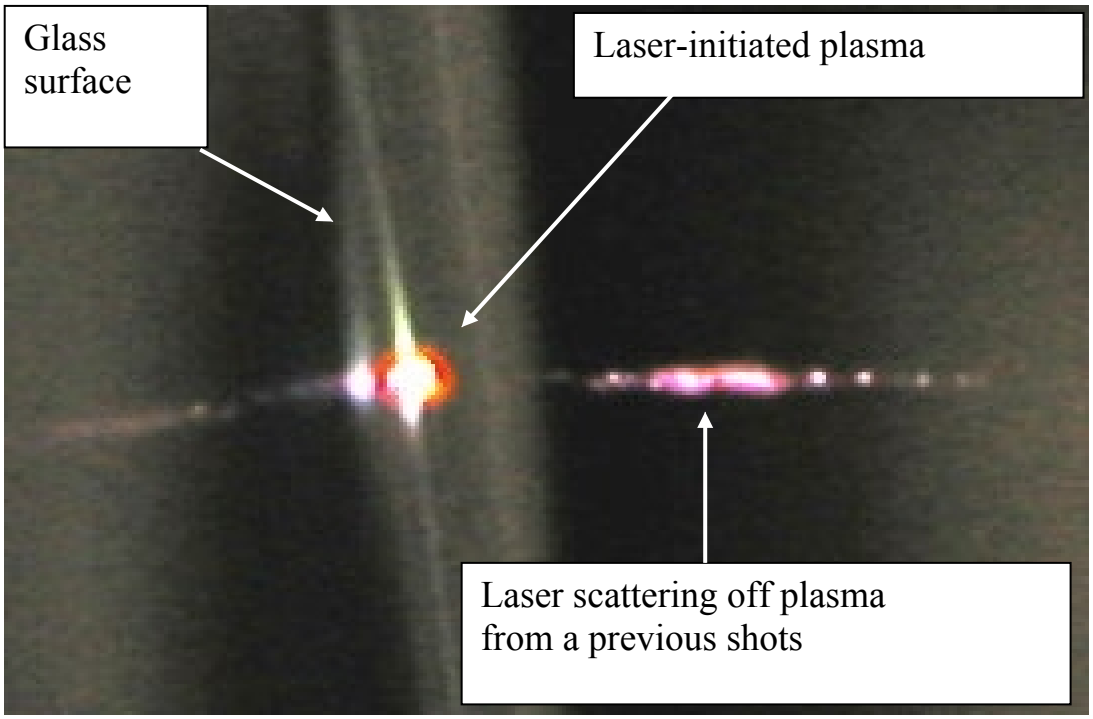

Figure 10. A high intensity, 50 fs, 800 nm USPL is focused onto a rotating disc of glass in this photograph. Continuum generation and recombination of ions and electrons produce the bright spot near the surface of the glass at the center of the plasma. Laser scattering off the ablated particles from previous pulses is also visible.

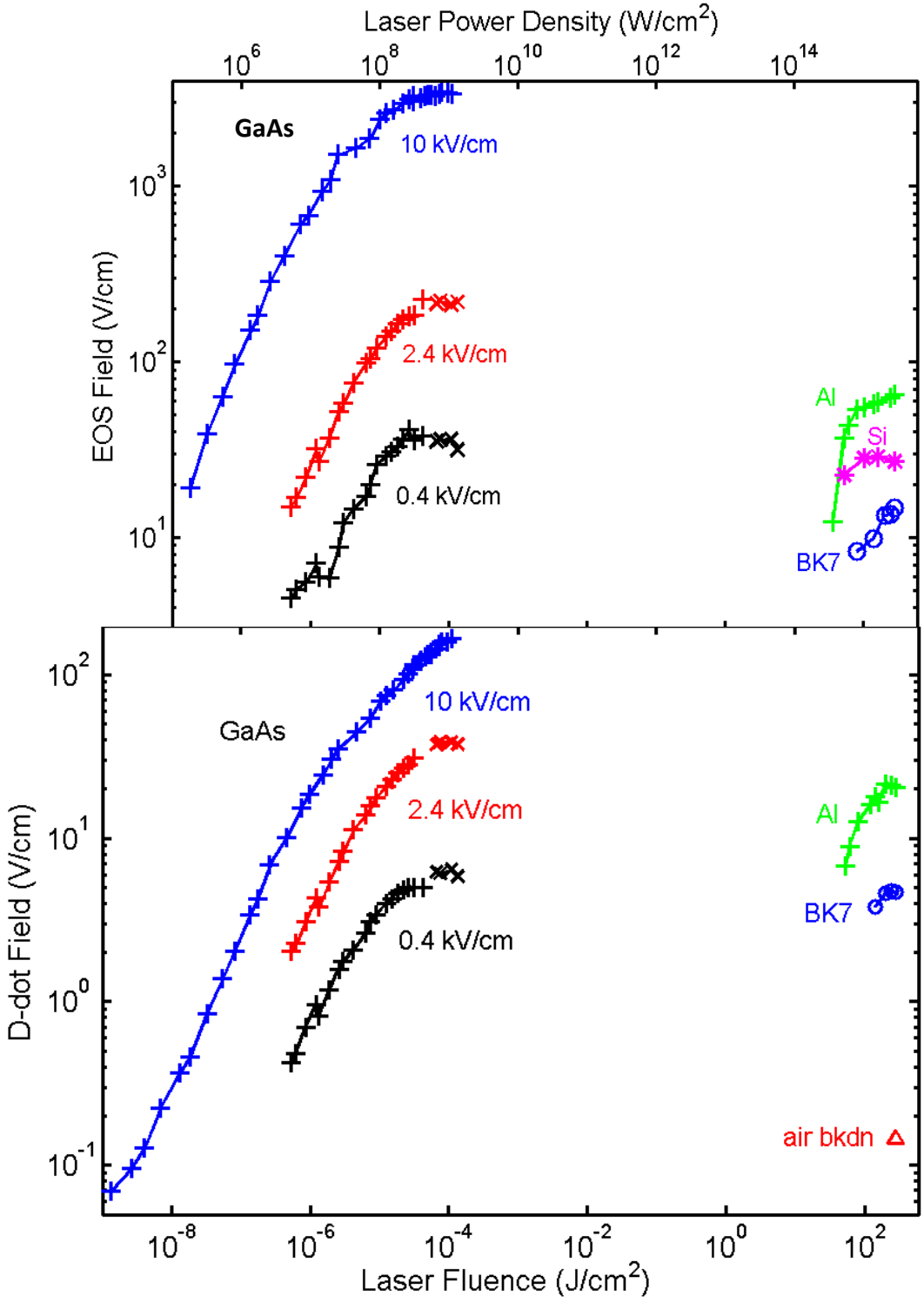

Figure 11. These plots show measurements of USPL-induced RF-THz as measured with 500 GHz BW EOS and a 65 GHz BW D-dot RF sensor. Peak-to-peak RF-THz electric fields were measured as a function of laser fluence or intensity for a GaAs PCSS at 3 applied fields and aluminum, silicon, BK7 (glass), and air with no applied field.

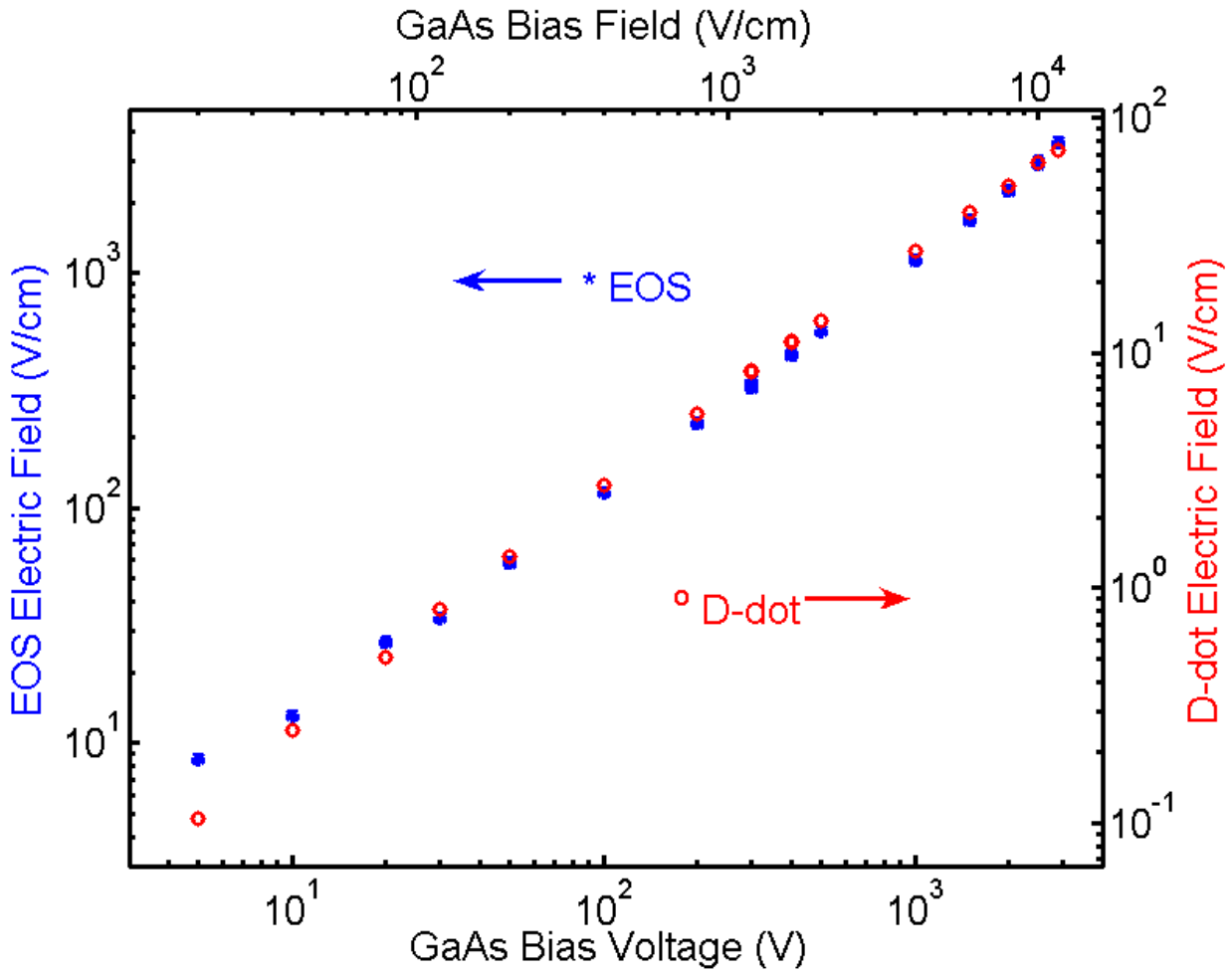

Figure 12. This plot shows very linear increase in the RF-THz radiation from a 100 fs USPL on GaAs as a function of the applied field. The signal was detected by both a D-dot RF monitor and EOS. The wider BW EOS sees more signal, but is less sensitive.

6. INITIAL THZ IMAGE DETECTION

The first discernible images from the THz system are shown in Figure 13. The shadows are difficult to see as the signal-to-noise for these images was less than 2:1.

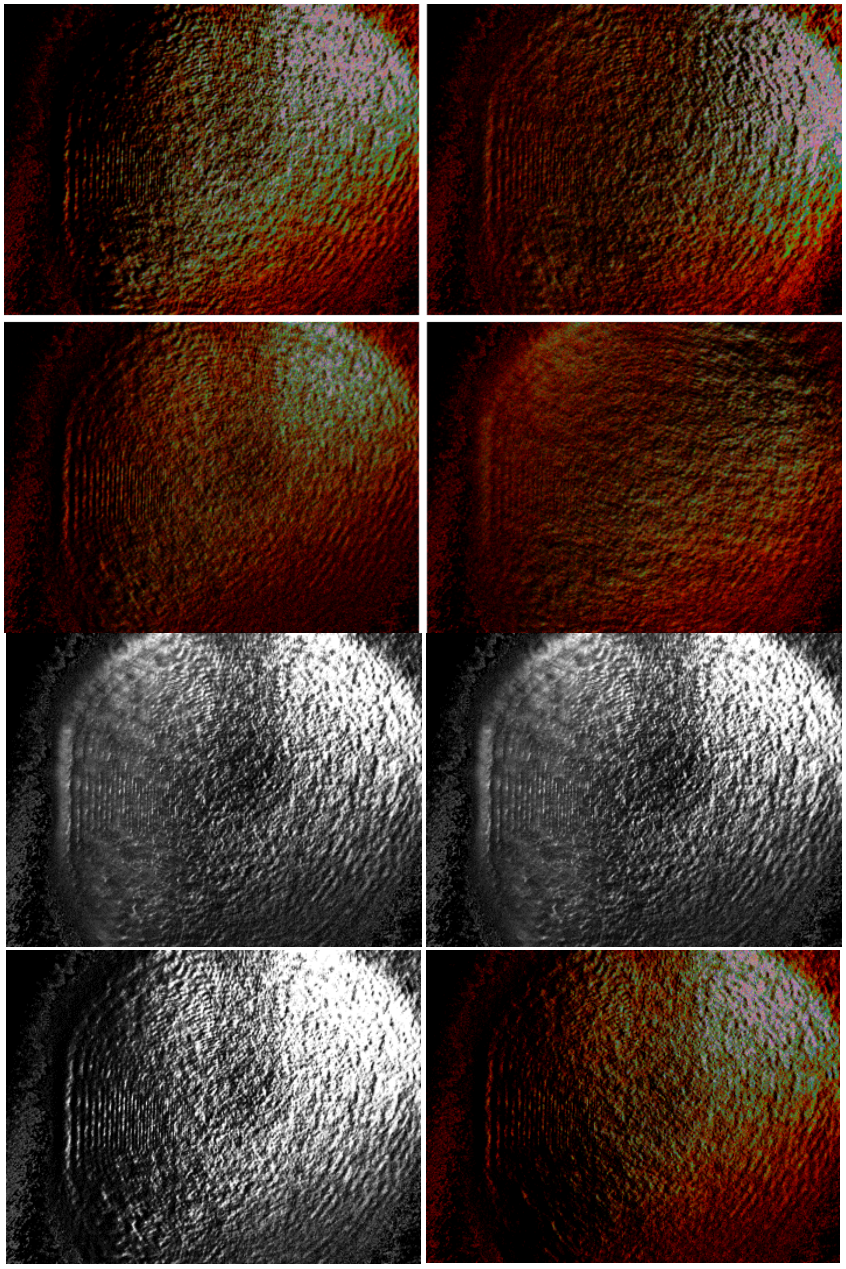

Figure 13. The top 2 images in the left column show a weak shadow of a ¼ inch metal post hanging from the top center of the photo. These were recorded after ninety 65 fs THz images were integrated in the camera before read-out. The top 2 images in the right show the same type of images without the THz radiation (background images). The bottom four images show the results of additional averaging (after internal averaging) with up to 60 selected signal and background images.

The contrast was improved by relay imaging the optical probe pulse from the EO crystal to the camera. This also provided magnification adjustment, to match the 1 cm^2 EO crystal to the focal plane of the camera. Unfortunately, this approach puts the EO crystal defects in the object focal plan, so that they are much more prominent than they were in previous images. Images of a smaller, tapered, inverted post using optical relay imaging are shown in Figure 14. The contrast between the shadow of the tapered post and the surrounding THz radiation is higher than in the images of the previous figure. However, the crystal defects showing in the middle of the shadow in the top two images are more noticeable than in previous images. The visibility of the defects appeared to drift in and out as images were collected, perhaps caused by slight variations in the laser profile between signal and background images

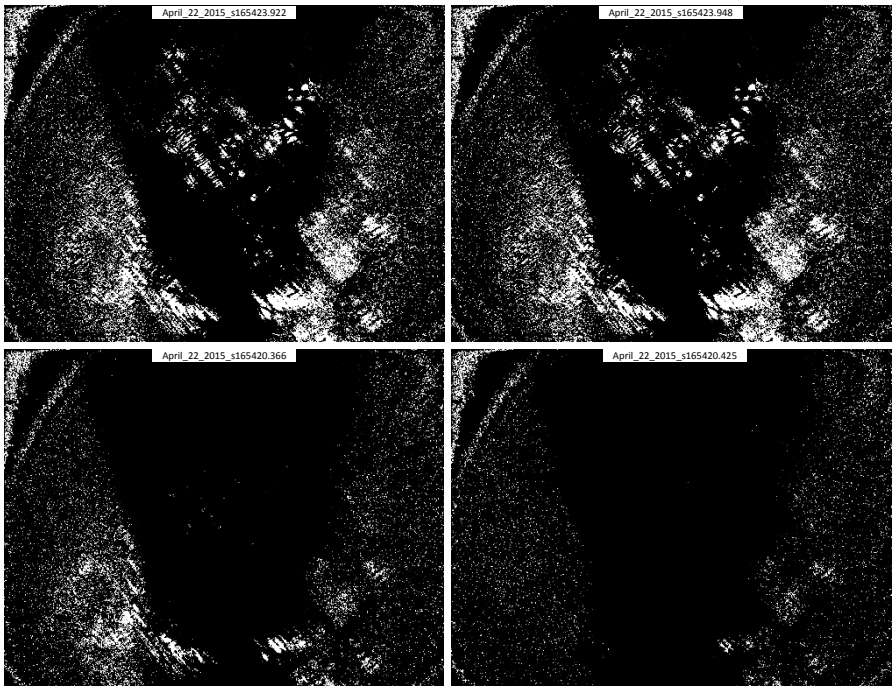

Figure 14. Higher magnification and contrast images of a smaller, tapered, inverted post were recorded after modifying the visible optics to relay image the EO crystal onto the camera.

7. IMAGING IMPROVEMENTS

After acquiring initial THz images with such low signal-to-noise ratios, the focus of this project turned to making changes that might increase signal or reduce the noise in the images. In this section many of the changes that were made and their results are described briefly.

7.1 Real time signal minus background images

A major improvement to the image acquisition system was the addition of double buffering saving "THz on" and "THz off" images as they are acquired. The image acquisition system can run free or synchronized to the THz imaging experiment. It initializes camera parameters, reads out data, processes data, displays data, and saves images to disk. The system was designed to take two successive data sets one signal and one background and subtract to display the difference. The system runs at a rate limited by the network card with frame rates up to 30Hz. The improved system became a valuable diagnostic rapidly showing the effects of making improvements in the experiment. One such improvement was mitigating the vibrational and acoustical effects of the pellicle beam combiner. The system helped minimize the disturbances from the pellicle beam combiner and showed the need to find an alternative substrate for the pellicle. The sound waves and air turbulence in the lab produced vibrations on the pellicle which generated major spatial variations on the probe beam intensity. This made it difficult to see the THz signal. The pellicle was replaced. See section "7.11. Silicon Beam Combiner".

7.2 System synchronized to 80 MHz seed laser

A second major improvement to system timing was the synchronization of all timing generators to the 80 MHz seed laser. The timing delay generators are locked to a sub-harmonic of the 80 MHz laser with internal phase lock loops. The design was integrated into the system architecture which made it easily modifiable and scalable. The system synchronizes two laser systems, diagnostics, the THz pulse charger, and the image acquisition from this single reference. This allows independent timing delay control of the laser systems with the ability to generate continuous synchronized events, single shot or burst mode. This system architecture is synchronized to 2 ps rms with less than 5 ps jitter in the seed laser. The 80 MHz reference is divided down to 1 kHz, which is further divided to 5 and 10 Hz. The slower signals are "ANDed" with the 1 kHz reference signal to generate the experimental signals for synchronized THz generation and data collection. Figures of the complete timing system can be seen in Figure 8 and Figure 9 of section "4. Timing: Laser, Pulser, Diagnostics, & Image Acquisition."

The two coupled systems work in tandem to synchronized hardware (timing system) and software(data system) to visualize the THz effect. The hardware synchronizes the timing for generating background and signal images, integration start times, controlling the readout period, controlling the save to disk period, controlling the THz high voltage pulser, and laser pulses. With the synchronized hardware the software arms the instruments, reads the images, image processes, takes the difference of the signal-background, scales the image intensity to a custom pseudo color scale, and displays the difference. The final report shows THz images of static thin metallic films. With the improvement of the new system the contrast improvements went from a signal to noise of 2:1 to 25:1.

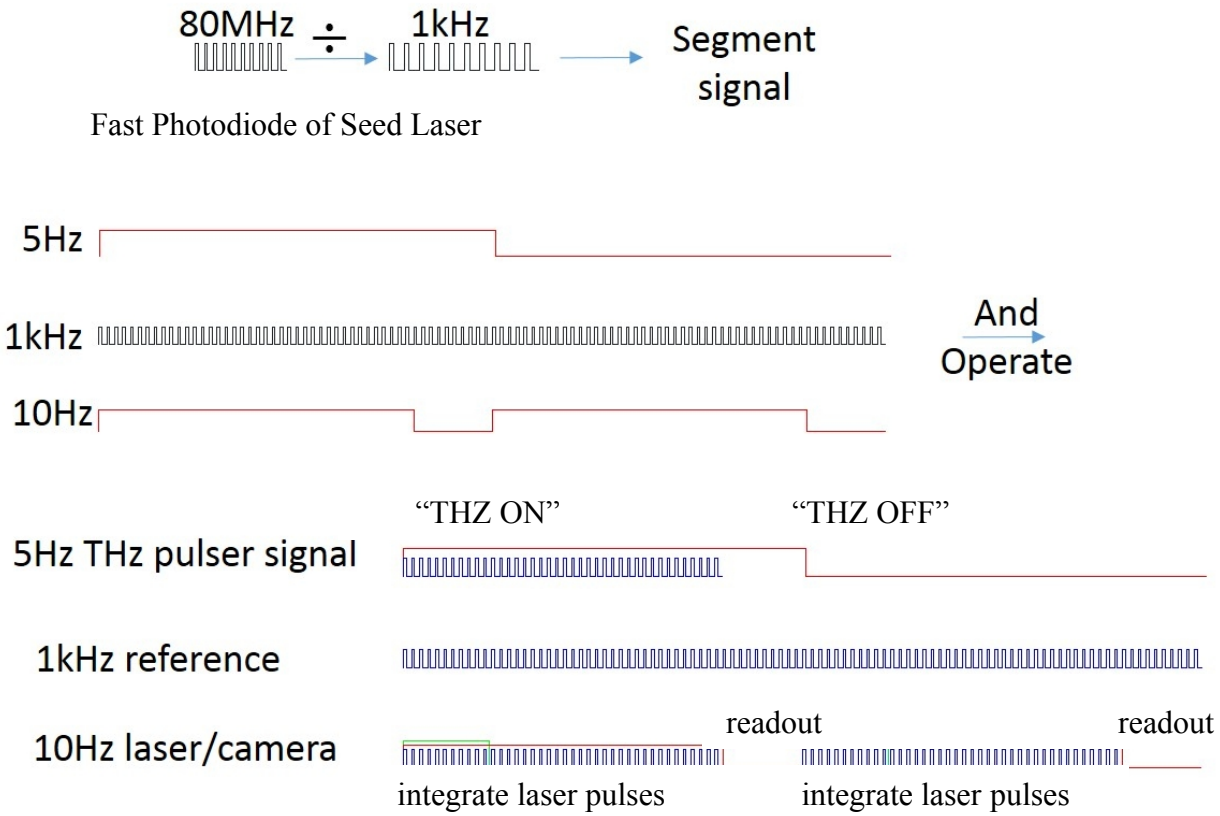

Figure 15. Division of the 80 MHz seed laser repletion rate is divided to create a 1 kHz reference signal. This reference is further divided to 5 and 10 Hz to create and buffer "THz on" and "THz off" images.

7.3. THz to visible image transfer and transport

Transferring the THz image information from the THz beam to the optical probe pulse in the EO crystal has two possibilities. If a THz image is formed in a thin EO crystal, then a parallel visible beam with spatial modulation from the THz image can be transported directly to the camera focal plane. This parallel beam can be expanded or compressed to match the size of the camera focal plane using two lenses. Alternatively, a diverging, converging, or scattered visible beam from the crystal can transport the spatial modulation to the camera focal plane by relay imaging the EO crystal onto the focal plane. As described in the previous section, the second approach improves contrast and can map the crystal to the size of the camera focal plane, but unfortunately, it also improves the visibility of the crystal defects. Both approaches are being tested for imaging (reflection) and shadowing (transmission).

7.4. Laser profile drift

If the laser intensity profile varies during the time between acquiring the signal image and acquiring the background image, the variation will remain in the image after the background is subtracted from the signal. This effect can be reduced by monitoring the laser profile and adjusting the laser alignment. It can also be reduced by minimizing the time between signal and background image acquisition.

7.5. Eliminate room light and THz source carrier recombination radiation

A narrow band notch filter (800 ± 25 nm) was placed in front of the camera to eliminate broad band room light outside this narrow band around the USPL (800 ± 10 nm). This filter also eliminates the 875 nm carrier recombination radiation from the GaAs THz source.

7.6. Eliminate 800 nm light reflected from the THz source

To eliminate reflection of the 800 nm laser trigger of the GaAs THz source, a dark colored sheet of polypropylene, which absorbs optical radiation while passing THz radiation, was placed between the THz source and the EO crystal. A plastic that absorbs 800 nm and transmits wide band THz was placed between after the OAP that collects the THz from the PCSS to eliminate reflection of the laser pulse from the PCSS into the EO crystal.

7.7. THz electro-magnetic interference (EMI) into camera

EMI from the THz signal may interfere with camera operation. This is checked by comparing the camera operation with THz on and THz off. If this becomes a problem, another pellicle may be used to reflect the visible into the camera and transmit the THz to a beam dump.

7.8. Camera noise: dark current, readout noise, and shot noise

Effects of camera dark current are reduced by decreasing camera integration time. This should not be significant until integration time is longer than a few seconds. Camera readout noise is typically a fixed level, so this effect can be reduced by increasing the camera signal near to saturation. This can be done either with longer integration time or increasing the visible probe pulse intensity. Shot noise is only significant a very low signal levels, so this is essentially eliminated by increasing the camera signal near to saturation.

7.9. Crystal defects

EO crystals with lower defect densities are desired. Unfortunately, using thicker crystals for more signal increases the number of defects. Relay imaging the optical image at the EO crystal to the focal plane of the camera puts them in the image focus and degrades the image contrast and quality.

7.10. Thicker EO Crystal

Thicker EO crystals provide more THz to visible conversion, but they also distort image transfer and provide more defects to distort the background subtraction (section “

7.11. CMOS Versus CCD Cameras

CMOS cameras are rapidly reducing their dark current and readout noise and increase their quantum efficiency compared to CCD cameras. A CMOS camera was tested and significant improvement was not observed.

7.12. Fast High Voltage Pulser for THz Source

A custom manufactured 50 ns rise time pulser was purchased to increase the applied field across the PCSS THz source. The previous pulser supplied 2.5 kV across the 2.5 mm long PCSS and the new pulser increased this to 5.5 kV (limited by surface flashover) and the THz signal increased by more than a factor of 2. A larger PCSS and laser beam will be tested up 10 kV, but the larger THz source will reduce the parallelism of the THz beam between OAP mirrors, which will degrade transmitted (shadowed) images.

7.11. Silicon Beam Combiner

The thin film pellicle originally used to combine the THz and visible probe beams was very sensitive to sound and air turbulence which distorted the probe beam. The thin film pellicle was replaced with a silicon beam combiner that is nearly transparent to the THz and has eliminated the pellicle vibrations.

7.14. Camera Signal Averaging and Probe Pulse Intensity

The signal recorded by the camera can be increased to near saturation by either increasing integration time or the intensity of the visible probe pulse. Test images were recorded when integrating over a 40 to 90 ms time interval and adjusting the visible probe pulse intensity to maintain roughly constant image counts. A significant change was not observed, so the shorter integration times are being used to reduce the time between signal and background acquisition.

7.15. Aperture THz Beam

A metallic aperture was placed in the THz beam between the OAP mirrors to be sure they were being overfilled with THz radiation and that a near parallel THz beam was obtained between the OAP mirrors.

7.16. 2X2 to 1 Pixel Binning

Since the wavelength of the THz radiation is much longer (30-300 μm) than the 800 nm visible probe beam, image resolution will be limited by diffraction of the THz and not by the pixel size in the camera (1 μm^2). The camera has the capability to increase signal and reduce readout time by binning nXn sets of pixels into a single readout unit up to n=8. This was tested with 2 X 2 binning which increased the signal by a factor of 4 and reduced the readout and disk writing time by a factor of 4. Higher density binning will be tested in the future.

8. IMAGES WITH IMPROVED SIGNAL-TO-NOISE

After making the improvements described in the previous sub-sections, "THz on" and "THz off" images were acquired and are shown as 3-dimensional intensity profiles in Figure 16.

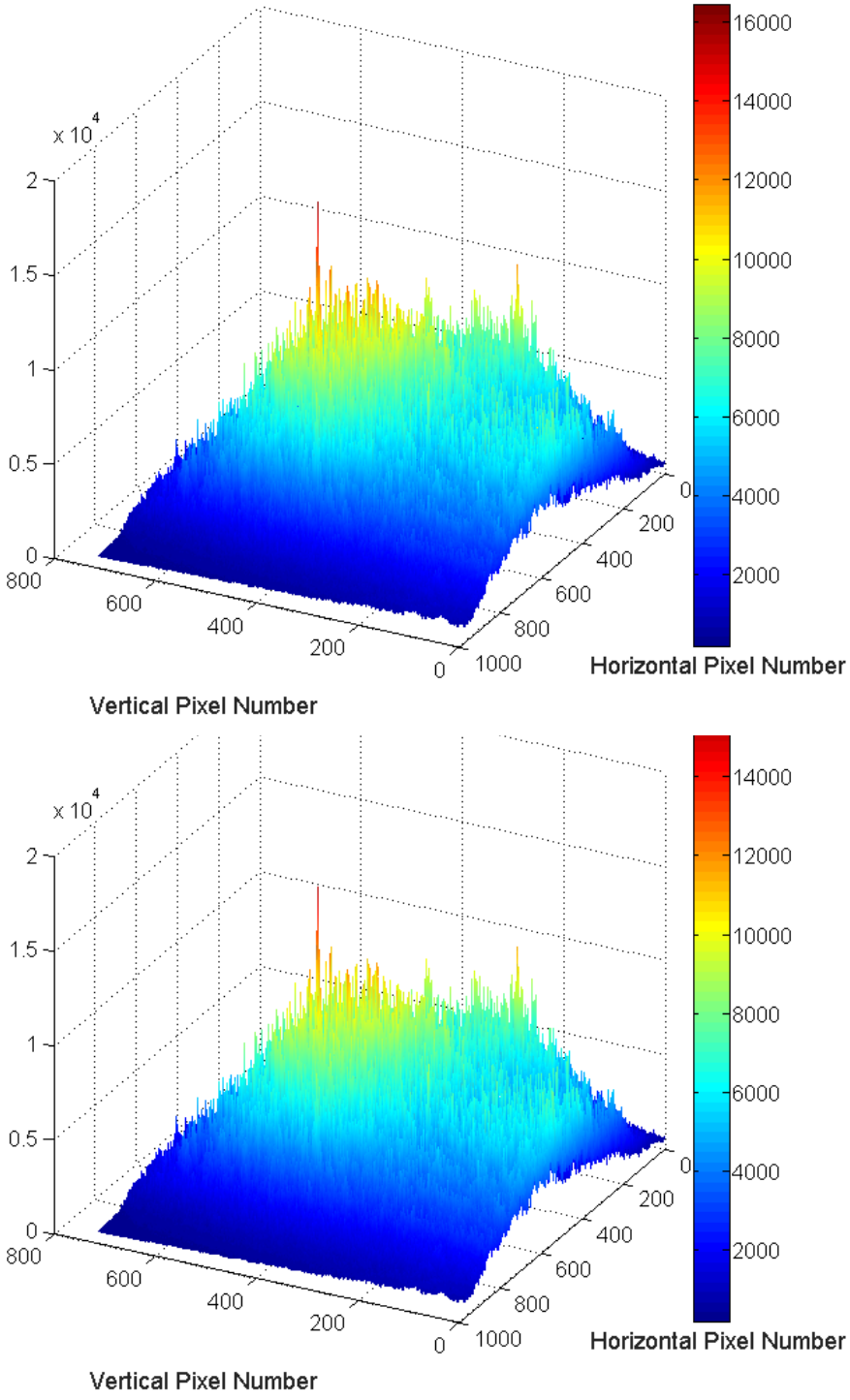

Figure 16. The "THz on" intensity profile (top) looks identical to the "THz off" profile (bottom) because their difference intensity shown in the next figure is only 2% of these images.

The difference profile "THz on" minus THz off" or signal minus background is shown in Figure 17. The signal and background images (Figure 16) were obtained by averaging approximately 50 camera frames with the THz pulse charger "on" and "off" recorded at 10 Hz. Each frame was recorded after collecting signal or background from 40 laser pulses at 1 kHz. The final difference image is the result of measurements from 4000 laser pulses (repetitions of the experiment).

The overwhelming positive value of the signal in the difference image demonstrates that this image is not noise. In fact, a close look at the boundaries of this image shows negative values of only ~10 counts. Since the peak signal is over 300 counts, this implies a signal to noise measurement of 30 to 1. Single shot measurements without averaging show a signal to noise ratio of only approximately 2 to 1, similar to the signal to noise measure with averaging in our initial images shown in section "6. Initial THz image detection".

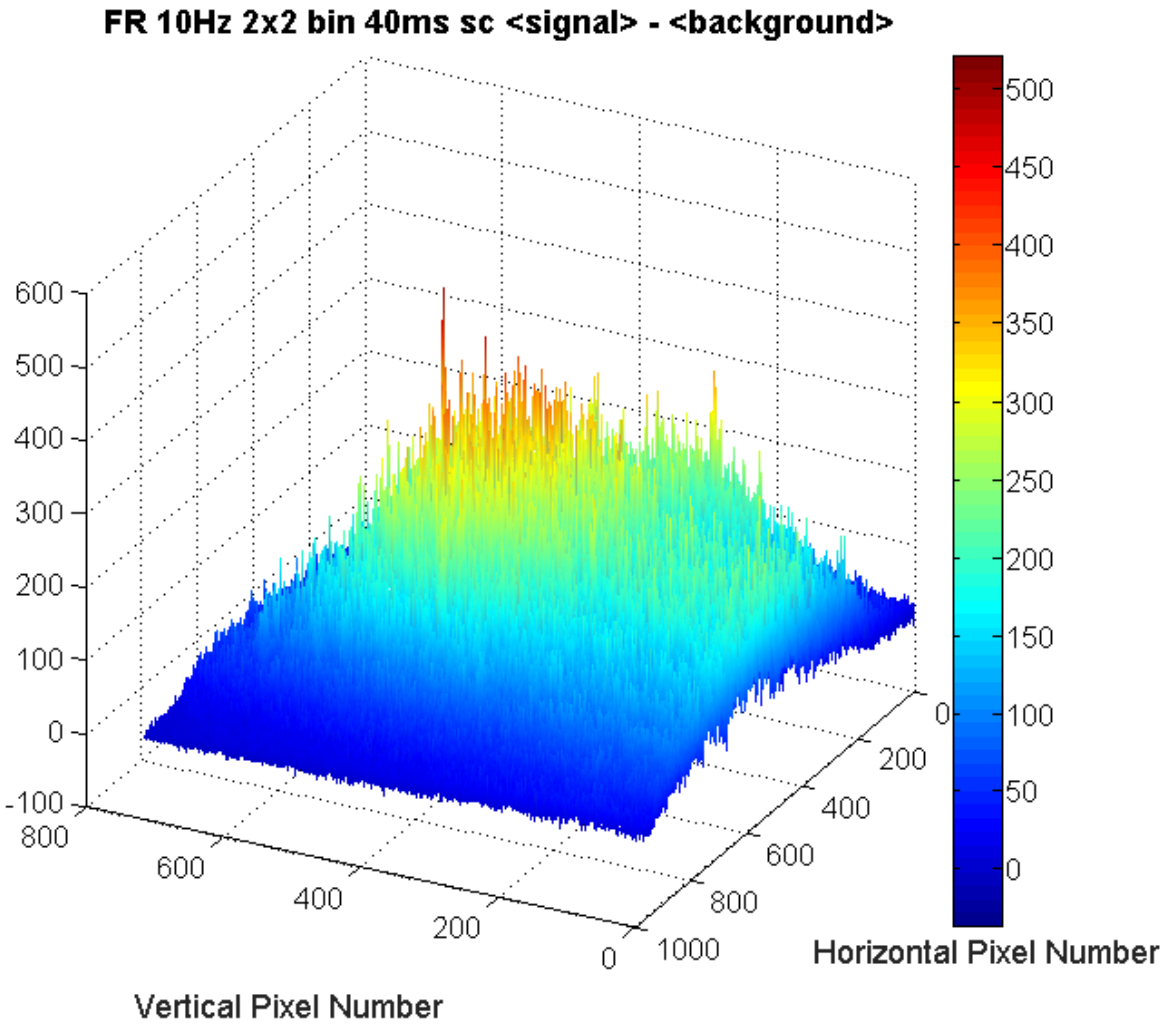

Figure 17. This difference of the images in the previous figure shows the THz signal which remains after subtracting the fixed background from the probe pulse through the EO crystal with no THz signal.

"THz on" and "THz off" images are shown as 2-dimensional false color images in Figure 18.

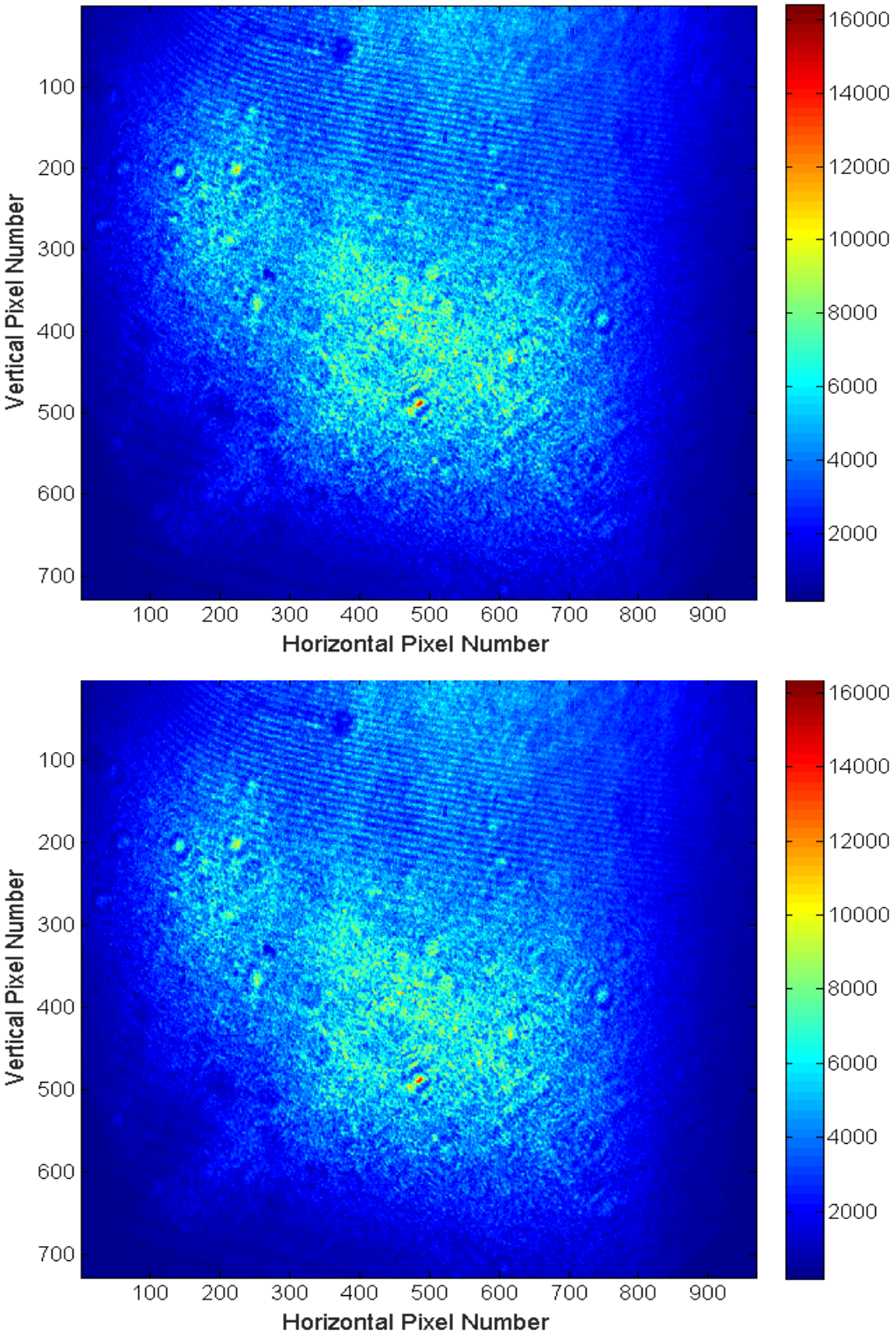

Figure 18. False color images of the "THz on" and "THz off" images are shown. These same images are shown as 3-dimensional profiles in Figure 16.

The difference image of "THZ on" and "THz off" is shown as 2-dimensional false color image in Figure 19. Except for the intensity of this image, it looks very similar to those in Figure 18.

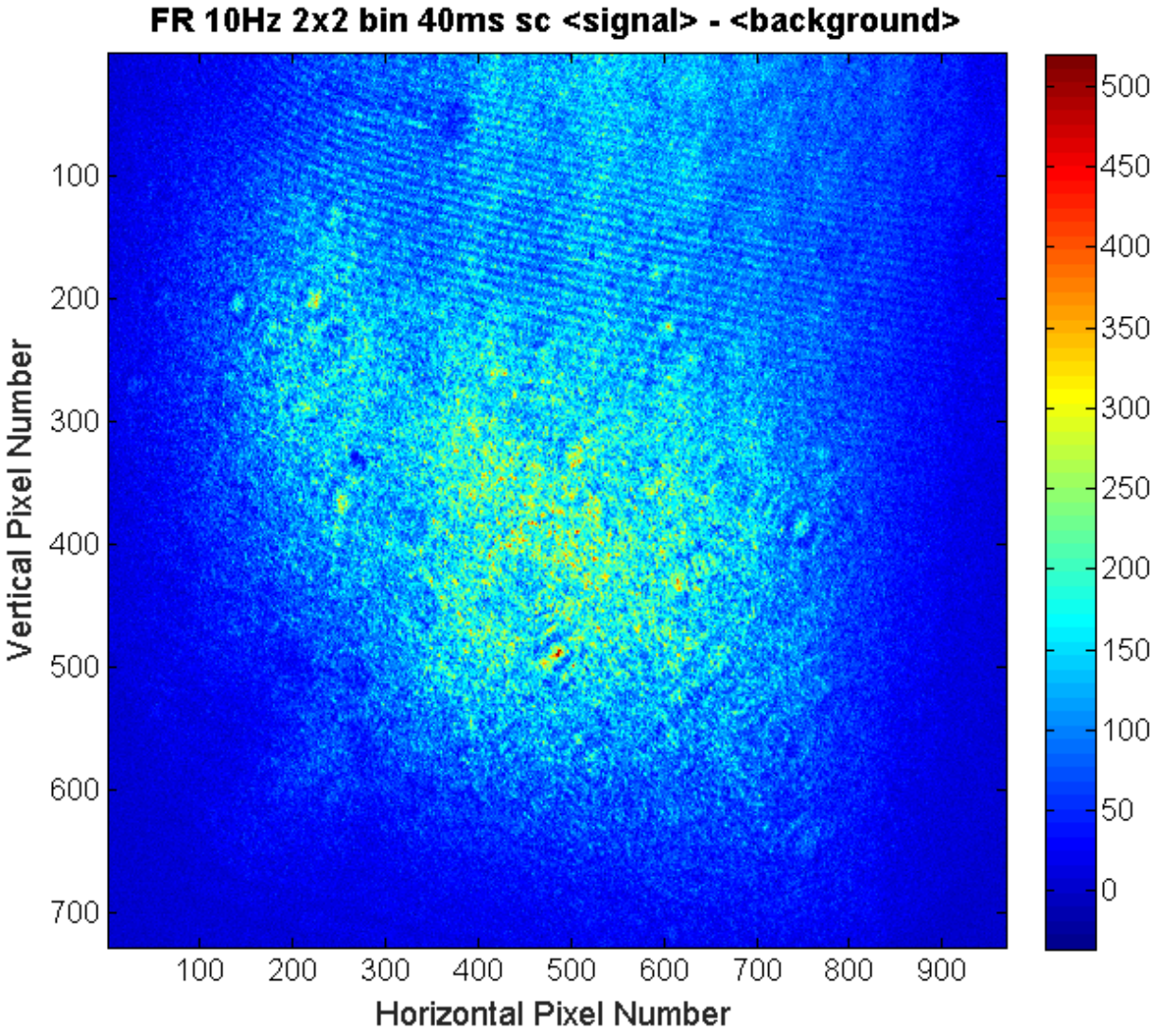

Figure 19. A false color difference image of the "THz on" and "THz off" images shows the image of the THz signal. This image is also shown as 3-dimensional profile in Figure 17.

9. THZ SHADOW OF FREE CARRIERS

A first test of THz interaction with materials containing nearly free electrons was performed by placing a thin aluminum shim in the THz beam between the collecting and focusing OAP mirrors. The nearly free electrons in the shim should completely absorb the THz. By placing the shim, so that it only blocked part of the THz beam, a shadow was observed. XXX and XXX show the shadow formed in the THz beam in a 3-dimensional profile and a 2-d false color image.

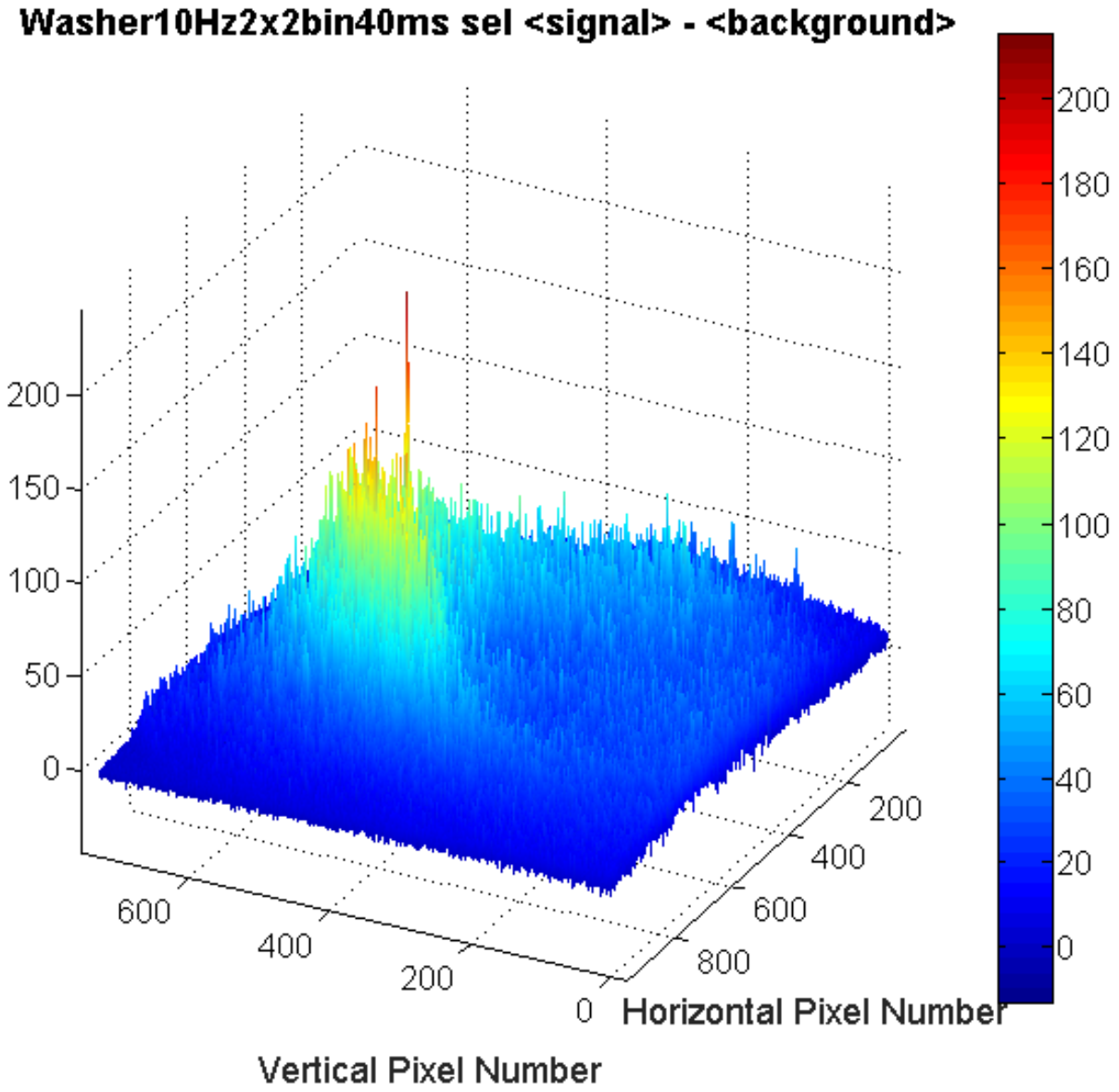

Figure 20. The shadow of a thin aluminum shim from the THz beam is shown on the right side of this 3-dimensional profile. This figure should be compared to the THz image without the shim shown in Figure 17.

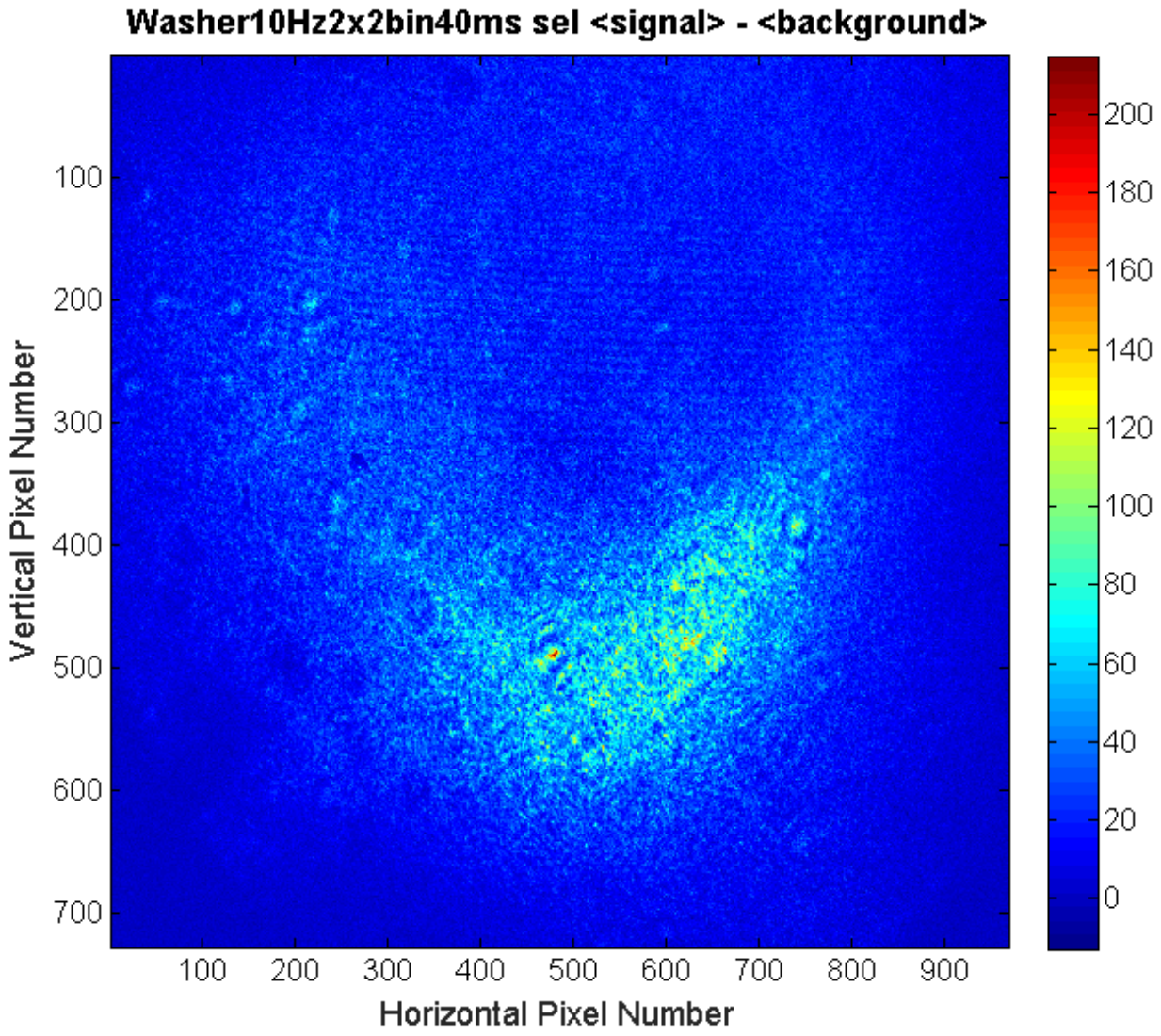

Figure 21. The shadow of a thin aluminum shim from the THz beam is shown on the top side of this 2-dimensional false color image. This figure should be compared to the THz image without the shim shown in Figure 19.

10. FUTURE IMPROVEMENTS IN INTENSITY AND CONTRAST

Several addition changes have been planned that may improve the intensity and contrast of the THz images. These changes and their potential benefits are described in the following sub-sections.

10.1. Normalize the difference image by the probe beam intensity

Since the polarization rotation in the EO crystal is proportional to the intensity of the 800 nm probe beam, a uniform spatial distribution of the intensity is desirable for showing only the spatial variation of the THz field. However, the probe beam spatial profile is Gaussian. In lieu of producing a more flat-topped beam, which may be attempted in the future, difference images may be improved by normalizing their intensity by the "THz off" signal, which is essentially the profile of the probe beam. Similarly, images of electrical breakdown or other phenomena using THz to illuminate the even may be eventually improved by normalizing the event image by the THz spatial distribution.

10.2. THz transmitted through the GaSs wafer

THz radiation is emitted from both surfaces of the GaAs wafer. The only difference in symmetry of the radiation paths, is that the carriers which radiate are created within 1 μm of the front (illuminated) surface of the 500 μm thick wafer, due to the extremely short absorption depth of above bandgap radiation in GaAs. This means THz emitted from the back side may have some absorption loss primarily due to defects in the GaAs wafer. These losses could be reduced by using a thinner GaAs wafer. Since THz absorption in GaAs is relatively weak, the radiation emitted from the back surface may be used as an alternative path from the THz source and may even have some practical advantages over the radiation from the front side.

10.3. Aperture the THz source

One advantage of back side THz emission is that it can be apertured without interfering with the incident laser that illuminates the front side. Ideally, an extended source cannot be transformed into a parallel beam with a lens. Even though the GaAs PCSS is only 2.5 mm square, radiation from this extended region cannot be transformed perfectly into a parallel beam. While a parallel beam is not required for illuminating and imaging an event with scattered light, it is important for illuminating and transporting a shadowed THz image created in transmission and for transferring the image from the THz beam to the probe beam in the EO crystal (section "7.3. THz to visible image transfer and transport"). The 2 inch diameter THz beam created with an OAP mirror may be used to produce shadows that must be demagnified to pass thru the 8 mm square cross-section of the EO crystal. The path length required to do this degrades the shadow, if it is being transported with a non-parallel beam of THz. On the other hand, a smaller PCSS will produce less THz power, since the USPL in this project has more than enough energy to saturate the THz radiation from the PCSS (Figure 11). Hence, there is an optimum diameter for the THz source to optimize the parallelism and power of the THz beam. To quantify this tradeoff, measurements will be made using an aperture on radiation from the back side of the GaAs wafer.

10.4. Parallel THz beam through the EO crystal

A nearly parallel THz beam in the EO crystal is important to transfer the image to the 800 nm probe beam due to the finite thickness of the crystal (section "7.3. THz to visible image transfer and transport"). Our present configuration uses one OAP mirror to collect the THz into a large parallel beam and a second OAP to concentrate it into the EO crystal. To create a parallel beam in the EO crystal, a third OAPs must be used compress the large parallel THz beam into a smaller parallel beam that will fit into the 8 mm square cross-section of the EO crystal. The diameter and focal length of this third OAP mirror are given by the speed of the second OPA mirror and the clear aperture of the EO crystal.

10.5. Transmission lenses compared to OAP mirrors

Transmission lenses made from silicon or polypropylene, which are transparent to wide band THz radiation may offer greater flexibility than OAP mirrors for improving THz imaging. Their disadvantage is a small amount of absorption of the THz radiation.

10.6. Buffer signal and background images before writing to disk

The present version of data acquisition software writes to disk after collecting either signal or background images. Thus there is an unnecessary disk writing time delay between collecting the signal and background images, which gives the spatial profile of the laser more time to drift. This time delay depends on the size of the image, but can be as large as 0.1 s (the number of pixels/80 MHz). Furthermore, the system software may occasionally interrupt the disk writing process and increase this delay by a pseudo-random amount. To avoid this delay between signal and background image pairs, separate buffers may be used to save both images before writing them to disk.

A further reduction in the time required for accumulating multiple signal and background image pairs can be achieved by buffering as many image pairs as possible in memory, before writing to disk. Since present-day computer memories are significantly larger than camera memories, it may be possible to acquire and store the entire image set in memory before writing to disk.

10.7. Record signal and background images simultaneously

An approach to acquire signal and background images uses two identical cameras to record two orthogonal polarizations of the 800 nm probe beam image. Taking the difference between these polarization images will provide the amount of polarization rotation and ideally, eliminate the fixed pattern noise. Both polarization images can be provided using a reflective polarizer or a Wollaston polarizing crystal. However, the exact alignment and magnification of both beam paths into the focal planes of both cameras and camera-to-camera gain and read-out variation more create or intensify more problems, than simultaneous imaging solves or reduces. The big advantage of this approach is that there would be no laser profile variation between the signal and background measurements. Even if multiple image pairs were required to reduce readout noise, the laser profiles for each signal minus background subtraction would be identical.

11. FOLLOW-ON PROJECT: WSEAT

Although the LDRD portion of the development of THz imaging has come to an end, multiple follow-on projects have been found to continue this work. One, Weapons Science Engineering and Technology (WSEAT), has the goal of imaging pre-breakdown phenomena to predict the probability of electrical breakdown during high voltage insult, such as a lightning strike during assembly, transport, or activation of critical system components. Such systems, often use lightning arrestor connectors (LACs) to short high voltage insults to ground at a predictable voltage [9]. Other projects have potential controlled access applications.

11.1. Laser-induced carriers in gallium silicon or gallium arsenide

The next step to image an electronic plasma distribution is to image photo-carriers and contact injected carriers in silicon or GaAs [12]. A first USPL pulse will create carriers in silicon with a recombination time of ~100 μs or GaAs with a recombination time of ~10 ns. Then second and third USPL pulses will generate THz radiation and resolve the THz image of nearly-free electrons and holes. This will be done first without an electric field to resolve dispersion of the photo-carriers, then with an applied electric field to resolve drift of the photo-carriers and injection of carries at the contacts. The advantage of developing THz image using photo-carriers in a semiconductor is the shot-to-shot reproducibility. These images should be very reproducible and not be washed-out with averaging.

11.2. Electrical breakdown imaging for WSEAT

The final goal of this project, to image electronic plasma during electrical breakdown, may be attained in WSEAT. A moderate voltage (10-20 kV), long pulse, electrical breakdown in air experiment will be set-up in the lab with the THz imaging experiment. The air gap will be pulsed with a variable rise time power supply to the approximate threshold for electric breakdown. A first USPL pulse will initiate electric breakdown and two subsequent pulses will create THz radiation and resolve the THz image from the electrical breakdown event as a function of delay time. Strong laser triggering will reduce the timing jitter of the electrical breakdown event and the impact of the laser on the observed pre-breakdown phenomena will be assessed by varying the intensity of the first USPL pulse. Repeatability and timing jitter of the electrical breakdown event will limit the time resolution of these measurements, not the 3 ps THz pulse. It remains to be seen how well pre-breakdown plasma distributions can be resolved with wide band THz radiation.

12. CONCLUSIONS

The initial steps for the development of ultra-short pulse laser (USPL) induced terahertz (THz) radiation to image electronic plasmas during electrical breakdown were taken during this project. Three USPL pulses were created from a seed laser and two chirped-pulse regenerative amplifiers with sub-picosecond timing resolution and picosecond jitter. Laser timing, optical diagnostics, THz source pulse charging, and signal minus background image acquisition were synchronized with multiple digital delay generators locked to the 80 MHz repetition rate of the seed laser. The generation of wide band THZ radiation was demonstrated with a USPL incident on a high voltage biased GaAs PCCS. Images of the emitted THz and shadows of metallic objects in the THz beam were resolved with electro-optic imaging (EOI) and acquired with a high gain, low noise digital camera. The timing and image acquisition were synchronized to produce real time signal minus background images as well as reduced-noise off-line signal averaged images. Over the course of this project, the signal to noise ratio of THz images was improved from less than 2 to greater than 30. Many of the improvements were described in this document and several others were proposed.

Fortunately, the development of this technology will not end with this project as multiple follow-on projects have been found to continue improvements and acquire images of high speed phenomena including electrical breakdown. In particular, the Weapons Science Engineering and Technology (WSEAT) program will continue to improve THz imaging and acquire THz images of the electronic plasma distributions associated with pre-breakdown phenomena [12,13]. These images will be used to develop and improve models of the probability of electrical breakdown in complicated electronic systems often protected by LACs [9].

13. REFERENCES

1. J. P. Brainard and L. Andrews, IEEE Trans. Compon., Hybrids, Manuf. Technol. 2, 309 (1979).

2. H. P. Hjalmarson, A. C. Pineda, R. E. Jorgenson and M. F. Pasik, 2011 PPC Proc., pg. 223.

3. Fredrick Wooten, *Optical Properties of Solids,* Academic Press, NY, 1972, pp 42-107.

4. Harold P. Hjalmarson, Fred J Zutavern, Jane M. Lehr, *Electrical Breakdown Phenomena Involving Material Interfaces (U),* SAND2013-5514C, Sandia National Laboratories, Albuquerque, NM (UUR), July 2013.

5. See for example: Daniel Mittleman (Ed.), Springer Series in Optical Sciences, Vol. 85, 2003, XVI.

6. Q. Wu, T. D. Hewitt, and X.C. Zhang, "Two dimensional electro-optic imaging of THz beams," Appl. Phys. Lett. 69, 1026 (1996)

7. Zhang Man, Pan Rui, Xiong Wei, He Ting, Shen Jing-Ling, "A Compressed Terahertz Imaging Method," Chin. Phys. Lett., 29, No. 10 104208 (2012)

8. Peiponen, Kai-Erik; Zeitler, Axel; Kuwata-Gonokami, Makoto (Eds.), THz Spectroscopy and Imaging, Springer, 2013, XXXI, 641 pp 302.

9. J. Slepian and W. F. Berkey, J. Appl. Phys. 11, 765 (1940).

10. Fred J Zutavern, James V. Rudd, Ray T. Collins, Jr., Leroy A. McPherson, Jr., Thomas R. Nelson, Ting S. Luk, and Stewart M. Cameron, "Free-Space, Electro-Optic Sampling and Remote Mapping of Electromagnetic Fields from Emitting Structures Using Femtosecond Terahertz Transceivers," SNL Report SAND2004-5378, Albuquerque, NM, March, 2004.

11. F. J Zutavern, S.F. Glover, A. Mar, M.J. Cich, G.M. Loubriel, M.E. Swalby, R.T. Collins, K.H. Greives, N.D. Keator, "High Current, Multi-Filament Photoconductive Semiconductor Switching," Proc. 17th IEEE Pulsed Power Conference, Chicago, June 2011.

12. F. J Zutavern, A. G. Baca, W. W. Chow, M. J. Hafich, H. P. Hjalmarson, G. M. Loubriel, A. Mar, M. W. O'Malley, L. D. Roose, and G. A. Vawter, "Electron-hole Plasmas in Semiconductors," Proc. Pulsed Power Plasma Science (13th IEEE Pulsed Power Conference combined with the 28th IEEE Conference on Plasma Science), Las Vegas, NM, June 2001, pp. 289-293.

13. Harold P. Hjalmarson, et al. , "Electrical Breakdown Phenomena Involving Material Interfaces," *Proc. 18th IEEE Pulsed Power Conference,* Chicago, June 2013.

DISTRIBUTION

qty	mail stop	name	organization
1	MS0828	Basil Hassan	01510 (electronic copy)
1	MS1152	Larry Schneider	01350 (electronic copy)
1	MS1152	Mike Dinallo	01352 (electronic copy)
1	MS1152	Roy Jorgenson	01352 (electronic copy)
1	MS1152	Steve Glover	01353 (electronic copy)
1	MS1152	Jarod Delhotal	01353 (electronic copy)
1	MS1152	Jason Neely	01353 (electronic copy)
1	MS1153	David Gardner	05444 (electronic copy)
1	MS1153	Fred Zutavern	05444 (electronic copy)
1	MS1153	Aaron VanTassle	05444 (electronic copy)
1	MS1153	James Gruetzner	05444 (electronic copy)
1	MS1153	Eric Zeek	05444 (electronic copy)
1	MS1153	Tony Marrujo	05444 (electronic copy)
1	MS1153	Junji Urajama	05444 (electronic copy)
1	MS1153	Ryan Law	05444 (electronic copy)
1	MS1153	Ray Collins	05444 (electronic copy)
1	MS1153	Kenn Greives	05444 (electronic copy)
1	MS1153	Daniel Mauch	05444 (electronic copy)
1	MS1153	Verle Bigman	05444 (electronic copy)
1	MS1153	Richard Gallegos	05444 (electronic copy)
1	MS1173	Alex Roesler	05440 (electronic copy)
1	MS1179	Harold Hjalmarson	01341 (electronic copy)
1	MS0899	Technical Library	09536 (electronic copy)
1	MS0359	D. Chavez, LDRD Office	01911 (electronic copy)


Sandia National Laboratories